REVIEW

Invited Contribution from Award Winners of the 21st National Electrochemistry Congress in 2023

Recent Advances in Solar Photo(electro)catalytic Nitrogen Fixation

Jun-Bo Ma [a], Sheng Lin [a], Zhiqun Lin [b], Lan Sun [a,*], Chang-Jian Lin [a,*]

[a] State Key Laboratory of Physical Chemistry of Solid Surfaces, Department of Chemistry, College of Chemistry and Chemical Engineering, Xiamen University, Xiamen 361005, Fujian, China
[b] Department of Chemical and Biomolecular Engineering, National University of Singapore, Singapore 117585, Singapore

Abstract

Ammonia (NH_3) is an essential chemical in modern society. It is currently produced in industry by the Haber-Bosch process using H_2 and N_2 as reactants in the presence of iron-based catalysts at high-temperature (400−600 °C) and extremely highpressure (20−40 MPa) conditions. However, its efficiency is limited to 10%−15%. At the same time, a large amount of energy is consumed, and CO_2 emission is inevitably. The development of a sustainable, clean, and environmentally friendly energy system represents a key strategy to address energy crisis and environmental pollution, ultimately aiming to achieve carbon neutrality. Within this framework, semiconductor photocatalytic nitrogen fixation leverages green and pollution-free solar energy to produce NH_3 — an essential chemical raw material. This innovative process offers a sustainable alternative to the conventional chemical NH_3 production method that involves tremendous energy consumption and environmental pollution. Herein, this review provides a comprehensive overview of the photo(electroc)catalytic nitrogen fixation reaction, covering influencing factor, experimental equipment of photocatalysis, electrocatalysis and photoelectrocatalysis, characteristics, and reaction mechanism. Particularly, recent advances in semiconductor photocatalyst, photo(electro)catalytic nitrogen fixation system, and photo(electro)catalytic nitrogen fixation mechanism are discussed. Future research directions in solar photo(electro) catalytic nitrogen fixation technology are also outlined.

Keywords: Solar energy; Photo(electro)catalysis; Nitrogen fixation

1. Introduction

Ammonia (NH_3), a crucial chemical product, has been widely used in agriculture, industry, and manufacturing, among other fields. With an average annual output of 20 billion tons, it plays a pivotal role in sustaining the survival and development of hundreds of millions of people globally. NH_3 serves as not only a vital nitrogen-containing fertilizer to meet the growing food demand of global population, but also an indispensable raw material for the synthesis of a variety of economically valuable chemical products. The development potential and inherent commodity properties of NH_3 energy underscores its significance as a key strategic resource, prompting nations worldwide to actively explore and study its applications. The notably high bond energy (941 $kJ \cdot mol^{-1}$) and ionic potential (15.0 eV) of N_2 molecules contribute to their classification as one of the most chemically

Received 1 December 2023; Received in revised form 2 January 2024; Accepted 5 January 2024
Available online 15 January 2024

* Corresponding author, Lan Sun, Tel: (86-592)2186862, E-mail address: sunlan@xmu.edu.cn.
* Corresponding author, Chang-Jian Lin, Tel: (86-592)2189354, E-mail address: cjlin@xmu.edu.cn.

https://doi.org/10.61558/2993-074X.3443

stable noble gases. Consequently, the hydrogenation of N_2 under normal temperature and pressure remains a challenging task. In nature, rhizobia demonstrates the ability to perform biological nitrogen fixation under ambient temperature and pressure, facilitated by nitrifying enzymes that feature FeMo, FeV or FeFe cofactors as catalytic active sites for N_2. However, the stability of nitrifying enzyme is susceptible to air content, leading to instability. Furthermore, the synthesized NH_3 yield falls significantly short of meeting the actual demand of people [1]. The inception of industrial-scale NH_3 production can be traced back to the development of the high-energy-density Haber-Bosch process in the early 20th century. In this process, N_2 and H_2 are amalgamated on the surface of Fe-based catalyst under rigorous conditions (400−500 °C and 200−300 atm) [2−6]. Notably, while this method overcomes N_2 activation kinetics, it comes at a significant cost, consuming 1%−2% of global energy supply. Meanwhile, it contributes to the accelerated depletion of non-renewable energy sources [7−9]. Additionally, the release of CO_2 during the preparation of reactive hydrogen through methane steam reforming further exacerbates the global greenhouse effect [10,11]. Consequently, there is a pressing need to seek green and low-consumption nitrogen fixation methods under mild conditions.

In this context, the utilization of photocatalytic technology to convert abundant solar energy into chemical energy, stored in the form of chemical bonds, represents an effective strategy to alleviate energy crisis and mitigate environmental pollution.

2. Photocatalytic nitrogen fixation reaction and influencing factors

2.1. Photocatalytic nitrogen fixation reaction

The synthesis of NH_3 by nitrogen reduction reaction (NRR) is a multi-step heterogeneous catalytic chemical reaction involving multiple electrons and protons [12]: (1) Adsorption and activation of N_2 molecules on the catalyst surface; (2) Association or dissociation of N_2 molecules; (3) Reduction addition of N_2 and H_2; (4) Desorption of reduction products on the catalyst surface. In the process of converting hydrogen and nitrogen into NH_3 (Eqn. (1)), the extremely large energy gap (22.9 eV) between the highest occupied molecular orbital and the lowest unoccupied molecular orbital as well as the extremely strong electron affinity (−1.8 eV) of N_2 molecules make the reaction difficult to take place under mild experimental conditions [13,14]. However, through exploring biological nitrogen fixation [15] in nitrogenase with ATP as the energy transfer carrier and FeMoS core cluster as the main N_2 binding site (Eqn. (2)), it is found that converting nitrogen to NH_3 under environmental conditions can be realized by constructing transition metal-diazine complex (such as Mo-N_2, Co-N_2, etc.) homogeneous catalysts with the participation of protons and electrons. The catalytic activity and stability of such catalysts still need to be improved, but it provides the possibility for artificial nitrogen fixation at normal temperature and pressure. At the same time, secondary energy sources such as solar energy and electric energy are combined to synthesize a variety of practical chemicals (such as H_2 [16], O_2 [17], H_2O_2 [18] and CO [19], etc.) through photocatalysis, electrocatalysis or photoelectrocatalysis under environmental conditions. In other words, the combination of renewable energy and chemical conversion systems offers an innovative and challenging alternative to the Haber-Bosch method for environmentally sustainable artificial nitrogen fixation. Up to now, some promising research results have been achieved in the fields of photocatalytic nitrogen fixation (g-C_3N_4 [20] and TiO_2 [21]), electrocatalytic nitrogen fixation (Fe_2O_3 [22] and CoP [23]) and photoelectrocatalytic nitrogen fixation (Cu_2O [24] and Nb-$SrTiO_3$ [25]), but NH_3 production is still not satisfactory. In order to realize high and stable nitrogen fixation efficiency, several problems in the NRR process still need to be solved.

$$N_2 + 3H_2 \rightarrow 2NH_3 \quad (1)$$

$$N_2 + 8H^+ + 8e^- + 16ATP \rightarrow 2NH_3 + H_2 + 16ADP + 16Pi \quad (2)$$

2.2. Factors affecting photo(electro)catalytic nitrogen fixation reaction

2.2.1. Light absorption properties and separation of photogenerated charge carriers

Energy band theory divides electron energy levels of semiconductors into conduction band, valence band and forbidden band. Therefore, photocatalytic or photoelectrocatalytic nitrogen fixation based on semiconductor materials must involve two processes: the generation of photogenerated carriers, and the separation and transfer of photogenerated electron-hole pairs [26]. When the band gap energy of the semiconductor material is less than 2.0 eV (that is, it can absorb visible light with wavelength greater than 600 nm), and its conduction band potential is more negative than the reduction potential of N_2 (0.092 V vs. NHE) and the valence band potential is more positive than the oxidation potential of H_2O (1.23 V vs. NHE)

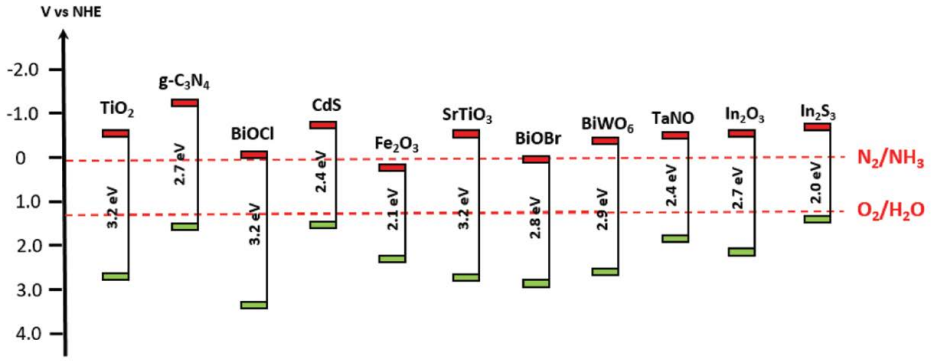

Fig. 1. Schematic diagram of the relationship between the energy band position of several common semiconductors and the reduction potential of nitrogen [29].

[27,28], this semiconductor can be considered as an ideal photocatalyst for nitrogen fixation. Fig. 1 illustrates the relationship between the band positions of several common semiconductors and the reduction potential of N_2. Obviously, the semiconductor with the best catalytic activity does not have a suitable band gap (E_g (TiO_2) = 3.2 eV, E_g (g-C_3N_4) = 2.7 eV). To this end, energy band structure control engineering, including doping [30], loading plasmon [31] and introducing lattice vacancy [32], is employed to enhance the light absorption of the catalyst to ensure high nitrogen fixation efficiency. Zhang et al. studied the effect of ultra-thin layered double hydroxide nanosheet photocatalysts (MII-MIII-LDH, MII = Mg, Zn, Ni, Cu; Effect of MIII = Cr, Al) on NRR response [33]. Among them, CuCr-LDH photocatalyst with controllable oxygen vacancy content synthesized by simple codeposition technology exhibits excellent photocatalytic nitrogen fixation activity at 500 nm because the introduction of oxygen vacancy induces the distortion of octahedral structure of MO_6. The photocatalytic NH_3 yield is 7.1 $\mu mol \cdot L^{-1}$, and the apparent quantum yield at 500 nm is 0.1%. Subsequently, they prepared ultra-thin anatase TiO_2 nanosheets with controllable number of oxygen vacancy through combining hydrothermal method with a simple Cu doping method [34]. The Cu-doped TiO_2 with 6% Cu doping has the optimum photocatalytic activity under full spectrum irradiation. The NH_3 yield can reach as high as 78.9 $\mu mol \cdot g^{-1} \cdot h^{-1}$, and the apparent quantum yield at 500 nm is 0.05%.

In addition, avoiding the recombination of photogenerated carriers is another key factor to ensure efficient nitrogen fixation. When the energy of the incident light is greater than or equal to the band gap of the semiconductor, the electrons in the valence band will be excited, and transit to the conduction band and release the holes in the valence band, thus producing photogenerated carriers with different charge properties. However, photogenerated electrons and holes tend to be recombined, and release energy in the bulk phase or on the surface of the semiconductor instead of reducing with adsorbed N_2 molecules [35], resulting in low photocatalytic nitrogen fixation efficiency. Therefore, the separation of photoelectron-hole pairs based on photoinduction is a necessary step for photocatalytic nitrogen fixation in semiconductor materials. Many researches indicate that developing nanostructured photocatalysts [36], loading cocatalysts [37], functional group modification [38], surface engineering [39] and heterogeneous structure construction [40] can effectively extend the lifetime of photogenerated carriers, thereby improving the photocatalytic NRR activity of samples.

2.2.2. *Adsorption and activation of N_2*

Heterogeneous catalytic reaction refers to the catalytic reaction that occurs at the interface of two phases, and is usually carried out on the surface of the catalyst. The adsorption and activation of reactive species on the catalyst surface are a prerequisite for effective catalysis. Accordingly, the construction of the active site on the catalyst surface is vital for the reaction induction. NRR is one of heterogeneous catalytic reactions, in which the adsorption and activation of N_2 molecules on the catalyst surface are a prerequisite for achieving artificial nitrogen fixation. In general, compared to photocatalysts with low surface area, photocatalysts with high specific surface area often show better photocatalytic activity for heterogeneous catalytic reactions such as hydrogen evolution reaction (HER) [41] and CO_2 conversion [42]. However, this is not the case for the NRR. Shiraishi et al. compared the effects of commercial TiO_2 catalysts with different surface areas on the NRR catalytic performance [43]. The TiO_2 sample with the largest surface area has the lowest NH_3 yield. It is clear that the specific surface area is not the key factor affecting the nitrogen fixation activity. The

high specific surface area can promote the physical adsorption between N_2 molecules and the catalyst, but the NRR gives more emphasis on improving the chemisorption between N_2 molecules and the catalyst. The coordination of N_2 molecules and the surface active site can effectively promote the dissociation of the N≡N triple bond and the electron transfer, and then increase the NH_3 yield [44]. Zhang et al. explored the effect of clean and complete surfaces of BiOCl with different crystal faces ((001) and (010)) on the chemisorption of N_2 molecules [45]. The results show that N_2 molecules adsorb on the surface of catalyst only through weak interaction. When oxygen vacancies are introduced into the (001) crystal plane of BiOCl, the formed vacancy state energy level can effectively capture the photogenerated electrons from the conduction band and transfer them to the π antibonding orbital of N_2 molecule, which avoids the recombination of photogenerated carriers, reduces the bond energy of N≡N triple bond, and thus promotes the adsorption and activation of N_2 molecule. N_2 molecules that obtain delocalized electrons from around oxygen vacancy have a further increased Lewis alkalinity, which is more conducive to subsequent hydrogenation reduction. Therefore, constructing oxygen vacancy on the catalyst surface is considered to be an effective structural engineering strategy. As a trapping center, oxygen vacancy can adsorb and activate inert gases such as O_2, N_2 and CO_2.

In addition to vacancy, doping levels introduced by ion doping, such as Fe^{3+} and Mo^{3+}, also has similar effects. Zhao et al. prepared Fe-doped $SrMoO_3$ by solvothermal method for photocatalytic nitrogen fixation [46]. Compared with undoped $SrMoO_3$, the band gap of Fe-doped samples is narrowed and the visible light response is enhanced. Furthermore, the Fe-Mo active centers formed by Fe and Mo coordination enhance the adsorption of N_2 molecules, and then promote the reduction of N_2 molecules.

Based on the above analysis, N_2 molecules, whether adsorbed at the vacancy site or doping site, will form metal-N_2 coordination compounds with surrounding metal atoms. Similar to the formation process of π bond, N_2 molecules and metal atoms enhance the adsorption of N_2 on the catalyst surface by sharing the lone pair electrons in the σ orbital [47,48]. The metal atoms then transfer the excess electrons from the orbital to the π antibonding orbital of N_2, reducing the bond energy of the N≡N triple bond and facilitating the dissociation of N_2. It is clear that the feedback electron transfer achieved in transition metal-N_2 coordination compounds provides the possibility for applying B, C, N doped non-metallic-N_2 coordination compounds in photo(electric)catalytic nitrogen fixation. Wang et al. prepared B-doped g-C_3N_4 (B/g-C_3N_4) for N_2 reduction [49]. The theoretical calculation shows that when N_2 molecules are adsorbed on the surface of B/g-C_3N_4 catalyst by the remote model and the side model, the bonding energies are 1.28 eV and 1.04 eV, respectively. N_2 molecules and the catalyst can achieve efficient nitrogen fixation at 0.2 V through the "accept-feedback" electron interaction. A good nitrogen fixing catalyst should be able to form a stable chemical bond with N_2 to achieve adsorption and activation of N_2.

2.2.3. HER as a competitive reaction

As a competitive reaction, HER is another major challenge in the process of photocatalytic NRR. Although the NRR is thermodynamically favorable, the HER involving two electron transfers is kinetically more dominant than the NRR involving six electron transfers (Eqn. (3)).

$$N_2 + 6H^+ + 6e^- \rightarrow 2NH_3 \ (E^\theta = 0.092 \text{ V vs. NHE}) \quad (3)$$

As mentioned above, a large amount of H_2 will still be produced in the process of biological nitrogen fixation even though nitrogenase is highly selective to NRR [50]. H_2 generation is one of the main factors affecting the biological nitrogen fixation efficiency. As a result, the selectivity of the reaction in the natural environment is still a key challenge in NRR process. However, in most artificial nitrogen fixation experimental systems rich in protic solvents, H^+ is easily adsorbed on the catalyst surface, which hinders the adsorption and dissociation of N_2 molecules, and thus HER is inevitable in NRR process. It is well known that the catalytic activity of reactions such as HER reaction and CO_2 reduction can be significantly improved by loading Pt, Rh, Ni and other metal-assisted catalysts on semiconductor surfaces [51−53]. However, the reaction efficiency of NRR is significantly inhibited by such metal-assisted catalysts. The photocatalytic nitrogen fixation activity of TiO_2 modified by different co-catalysts (Pt, Rh, Ru, Pd) was studied [54]. The NH_3 yield depends on the bonding strength between metal-cocatalyst and H atoms adsorbed on the surface. The stronger the bonding strength of M−H, the higher the NH_3 yield. At the same time, metal Ru not only enhances the light absorption as an electron catcher, but also effectively stabilizes the H atoms adsorbed on the metal surface, and thus increases NH_3 yield. In addition, a large number of theoretical and experimental studies have turned from doping

single metal to constructing heterogeneous electrocatalysts to improve the electrocatalytic NRR activity. For example, metal oxides and metal nitrides represented by CeO_x and VN containing defective states can significantly inhibit the adsorption of H atoms to enhance the selectivity of NRR [55]. Doping pre-transition metal atoms or using aprotic solvent for NH_3 synthesis can also effectively reduce the HER activity. The design of semiconductor surface structure engineering based on the creation of ion vacancy and doping site, the construction of complex heterojunction or the modification of N_2 active co-catalyst is an effective method to promote the adsorption and activation of N_2, and can inhibit the generation of H_2 [56].

2.2.4. Side reactions and products

N is an important element with multiple valence states, and its compounds have been widely used in all aspects of life. However, in the process of catalytic NRR, the formation of byproduct hydrazine (N_2H_4) and further oxidation of the target product [57] (Eqn. (4)) will reduce the NH_3 yield. In the experiment of photocatalytic nitrogen fixation, sacrificial agent is often added to avoid the formations of nitrate and nitrite at the cost of increasing the experimental cost. In electrocatalytic or photocatalytic nitrogen fixation experiments, photoelectrochemical cells with proton exchange membranes are often employed to achieve spatial separation of oxidation products and reduction products, thereby inhibiting the oxidation reaction of NH_3 [58].

$$2NH^{4+} + 3O_2 + 2h^+ \rightarrow NO_2^- + NO_3^- + 4H^+ + 2H_2O \quad (4)$$

3. Experimental apparatus and characteristics of photo(electro)catalytic nitrogen fixation reaction

With the deep understanding of the NRR mechanism and the continuous innovation of micro-nano synthesis technology in the field of catalysis, various nitrogen fixation catalysts have been synthesized, which also created the diverse and novel nitrogen fixation approaches and experimental devices. Based on this, the mainstream nitrogen fixation methods are divided into three categories: photocatalysis, electrocatalysis and photoelectrocatalysis. NRR on the surface of heterogeneous catalysts at ambient temperature and pressure has attracted great interest of researchers. Understanding experimental devices and reaction characteristics will facilitate the design and assembly of nitrogen fixation catalysts as well as the construction and optimization of experimental conditions to achieve efficient and stable nitrogen fixation.

3.1. Photocatalytic nitrogen fixation

In 1977, Schrauzer and Guth successfully achieved the photocatalytic hydrogenation reduction of N_2 through using Fe-doped anatase TiO_2 powder as the catalyst for NRR under ultraviolet irradiation for the first time [59], which opens a new direction in photocatalytic nitrogen fixation. Since then, a great deal of research work has been carried out to develop new photocatalysts for artificial nitrogen fixation [60–64]. In the photocatalytic nitrogen fixing system with solar energy as the reaction driving force, a quartz photochemical cell with good light transmittance has become the first choice of experimental equipment. A simple experimental device for photocatalytic nitrogen fixation is shown in Fig. 2, and its reaction process is as follows:

$$\text{Semiconductor} + h\nu \rightarrow e^- + h^+ \quad (5)$$

$$N_2 + 6H^+ + 6e^- \rightarrow 2NH_3 \quad (6)$$

$$2H_2O + 4h^+ \rightarrow O_2 + 4H^+ \quad (7)$$

First, the semiconductor is stimulated by light to produce photogenerated electron-holes (Eqn. (5)). Then, the photogenerated electron-hole is separated and transferred to the active sites on the surface. Finally, the photogenerated electrons and holes react with N_2 and H_2O adsorbed on the semiconductor surface to product NH_3 (Eqn. (6)) and O_2 (Eqn. (7)), respectively. It is unavoidable in

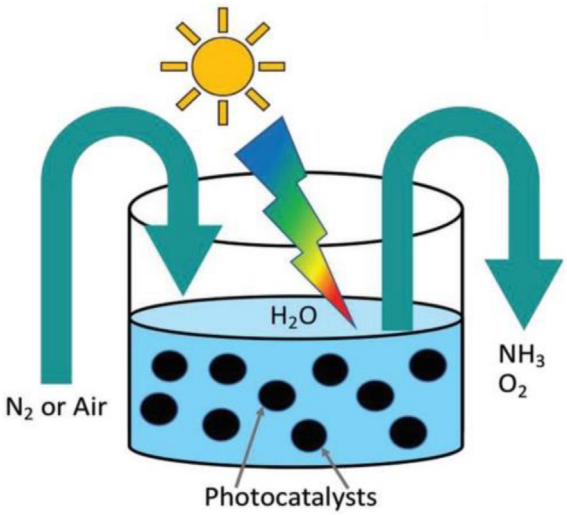

Fig. 2. Schematic diagram of experimental setup for photocatalytic nitrogen fixation [65].

photocatalytic nitrogen fixation experiments that NRR and oxygen evolution reaction (OER) occur simultaneously in the same system. Although there are still some problems in the reaction process such as catalyst inactivation and powder recovery, photocatalytic nitrogen fixation is still expected due to its simplicity and environmental protection.

3.2. Electrocatalytic nitrogen fixation

The earliest electrochemical synthesis of NH_3 can be traced back to the 1960s. Van Tamelen et al. proposed to use an aluminium anode and a nickel-chromium alloy cathode as the double electrodes for the electrolytic reduction of N_2 in a unipolar chamber containing 1, 2-dimethoxyethane solution of titanium tetrisopropanol, naphthalene, tetrabutylammonium chloride and aluminum isopropanol [66]. Since the aluminium anode is easily hydrolyzed and consumed after being converted to AlN, this method is not suitable for long-term reactions and large-scale production. To date, different kinds of electrochemical cells have been developed using liquid or solid electrolytes. According to the different reaction devices, the common nitrogen-fixing electrolytic cells can be divided into four categories: single chamber electrolytic cell, double chamber electrolytic cell, back-to-back electrolytic cell and polymer electrolyte membrane (PEM) cell. Fig. 3 illustrates the schematic diagram of four kinds of electrolytic cells. Among them, single-chamber cell and double-chamber cell are most commonly used.

3.2.1. Single-chamber electrolytic cell

A solid electrolyte with good proton or ion conductivity combined with a single chamber electrolytic cell (Fig. 3a) was used as an early experimental device for electrochemical nitrogen fixation at high temperature. In 1998, a solid electrolyte single chamber electrolytic cell was used to synthesize NH_3 under atmospheric pressure [68]. The H_2 was first converted into H^+ ion at the anode, and then high H^+ flux was obtained at 570 °C. Subsequently, H^+ was transferred to the cathode through the $SrCe_{0.95}Yb_{0.05}O_3$ solid electrolyte to participate in the reduction reaction. Limited by the high temperature from consuming fossil fuels and the easy

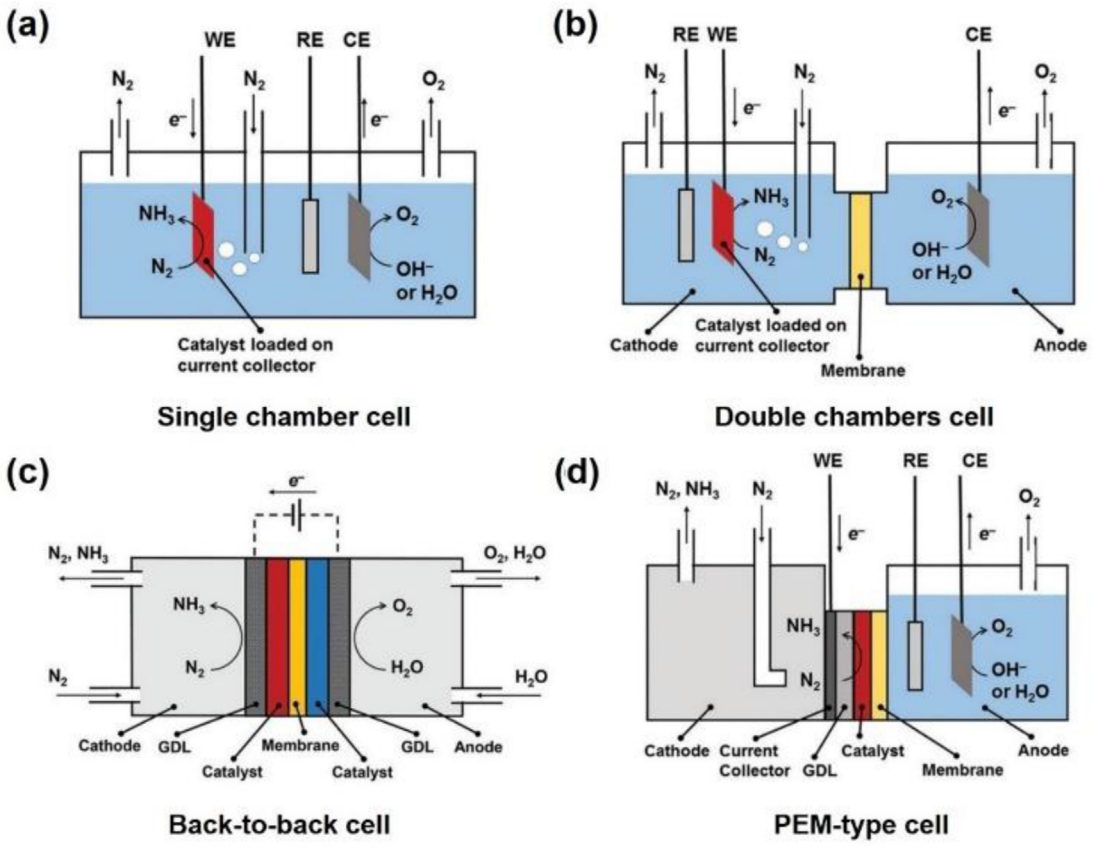

Fig. 3. Schematic diagram of experimental setup for electrocatalytic nitrogen fixation ((a) single chamber, (b) double chambers, (c) back-to-back and (d) PEM-type) [67].

decomposition of NH_3, this method was not applied in large-scale practice. After that, in order to reduce the reaction temperature, the experimental conditions were optimized [69], but it still could not achieve the purpose of nitrogen fixation at room temperature. In recent years, NRR in a single chamber electrolytic cell containing liquid electrolyte solutions has attracted extensive attention, and the composition of electrolyte solutions also involves different types including acid, basic and neutral salts. In 2018, Schechter et al. used RuPt/C as an electrocatalyst to synthesize NH_3 in 1.0 $mol \cdot L^{-1}$ NaOH solution. The NH_3 yield at −0.123 V was as high as 5.1×10^{-9} $g \cdot cm^{-2} \cdot h^{-1}$, and Faradaic efficiency was 13.2 % [70]. In 2019, Han et al. synthesized Au@CeO_2 electrocatalyst and carried out NRR in a single chamber electrolytic cell with 0.01 $mol \cdot L^{-1}$ H_2SO_4 as the electrolyte [71]. The NH_3 yield and Faradaic efficiency at −0.4 V were 28.2 $\mu g \cdot cm^{-2} \cdot h^{-1}$ and 9.5%, respectively. Because different types of electrocatalysts have their own advantages and disadvantages, it is difficult to determine the optimum pH of electrolyte for electrocatalytic nitrogen fixation. The acidic electrolyte solution provides abundant H^+ for hydrogenation of NRR, but also aggravates HER. Feng et al. reported that phosphate buffer (PBS) was more beneficial to artificial nitrogen fixation by inhibiting HER than H_2SO_4 and NaOH solutions [72]. Therefore, electrolytes need to be optimized according to the specific reaction system and catalyst. In addition, an ionic liquid, as a special liquid electrolyte, has been used to improve the Faradaic efficiency and NH_3 yield of electrocatalytic NRR because of its high N_2 solubility, involatility and stability. Single chamber electrolytic cell was widely used in the early exploration experiments of electrocatalytic NRR, but single experimental conditions (reaction atmosphere, medium, temperature) and diffusion oxidation of products would lead to the decrease of NRR efficiency. Therefore, the two-chamber electrolytic cell with complex structure and higher efficiency has become the best alternative for electrocatalytic nitrogen fixation.

3.2.2. Double-chamber electrolytic cell

In a single chamber electrolytic cell, oxidation reaction and reduction reaction occur in the same system at the same time. O_2 generated by the decomposition of H_2O on the anode surface tends to further oxidize NH_3 products, resulting in low reaction efficiency. In contrast, the two-chamber electrolytic cell which realizes the separation of cathode and anode spatially, is an effective method to solve the shortcoming of the single chamber electrolytic cell and improve the catalytic performance of NRR. A double chamber electrolytic cell separated by a proton exchange membrane (PEM) or an anion exchange membrane (AEM) is also called an H-type cell (Fig. 3b) due to its shape like an "H". The working electrode loading a catalyst and commercial reference electrodes such as Ag/AgCl and Hg/Hg_2Cl_2 are usually fixed in the cathode chamber, while inert electrodes such as Pt sheet and C rod are used as auxiliary electrodes in the anode chamber. During the reaction process, the H^+ or OH^- produced in the anode chamber is transferred to the cathode chamber through the proton exchange membrane or anion exchange membrane to participate in the NRR. Meanwhile, NH_3 in the form of NH^{4+} in the aqueous solution cannot pass through the exchange membrane, thus avoiding the reoxidation of the product. Recently, Ding et al. demonstrated that the conversion from N_2 to NH_3 under environmental conditions in an H-type electrolytic cell separated by Nafion 117 membrane was achieved with Fe-doped SnO_2 nanoparticles as a catalyst [73]. The NH_3 yield and Faradaic efficiency at −0.3 V in 0.1 $mol \cdot L^{-1}$ HCl were 82.7 $\mu g \cdot mg \cdot cat^{-1} \cdot h^{-1}$ and 20.4%, respectively. In addition, the different electrolytes in the cathode and cathode chambers can be chosen due to the blocking effect of the membrane, which provides greater freedom for the choice of experimental conditions. Kim constructed a double-electrolyte reaction device using LiCl/ethylenediamine (EDA) as the cathode electrolyte and H_2SO_4 solution as the anode electrolyte [74]. The Faradaic efficiency was increased by 17.2% because the synergistic effect of EDA electrolyte avoids H^+ loss caused by HER reaction compared with 2-propanol.

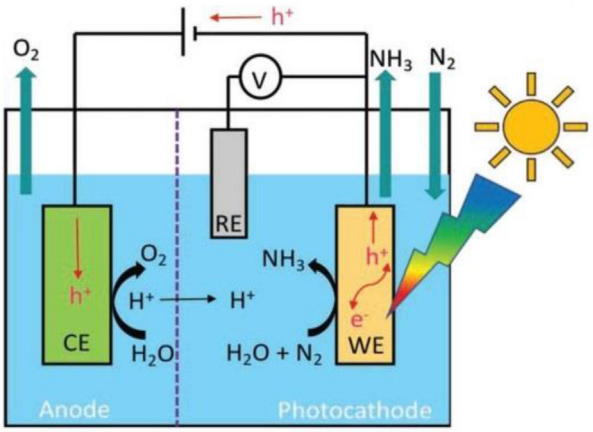

Fig. 4. Schematic diagram of experimental setup for photoelectrocatalytic nitrogen fixation [65].

3.3. Photoelectrocatalytic nitrogen fixation

Unlike the photocatalytic system in which powders are dispersed in a solution, photocatalysts are often made into electrodes used in photoelectrochemical cells. A classical photoelectrochemical reaction system is a three-electrode system, which is composed of a light source, a reaction cell, a working electrode modified by a catalyst, an auxiliary electrode and a reference electrode. Single chamber electrolytic cell [75] or double chamber electrolytic cell [76] are usually used as experimental devices for photoelectrocatalytic NRR. Fig. 4 shows a simple photoelectrocatalytic nitrogen fixation experimental device. Photoelectrocatalytic system combines the advantages of photocatalytic system and electrocatalytic system. Compared with electrocatalytic system, photoelectrocatalytic system can utilize solar energy as the reaction driving force, which greatly reduces the consumption of electric energy. Compared with photocatalysis, photoelectrocatalysis realizes the spatial separation of reaction products and effectively avoids the oxidation of NH_3. Besides, the additional bias promotes the separation and transfer of photogenerated carriers, which enhances the catalytic activity and reaction efficiency of NRR. Recently, Zhang et al. constructed N_v-g-C_3N_5/BiOBr p-n heterojunction by introducing nitrogen vacancy on g-C_3N_5 and then combining with BiOBr for photoelectrocatalytic nitrogen fixation [77]. The introduction of nitrogen vacancy narrowed the band gap of g-C_3N_5, enhanced light absorption, and transferred electrons from g-C_3N_5 conduction band to N_2 molecules adsorbed on the catalyst surface for activation. Moreover, the p-n heterojunction between g-C_3N_5 and BiOBr reduces the recombination of photogenerated carriers, and prolongs the lifetime of photogenerated electrons and holes. The NH_3 yield can reach 29.4 $\mu g \cdot h^{-1} \cdot mg^{-1}$ in the H-type electrolytic cell with a mixed solution of 0.5 $mol \cdot L^{-1}$ HCl and Na_2SO_4 as the electrolyte solution at −0.2 V. The wide range of experimental device and the diversity of catalysts encourage people to explore the NRR steadily.

4. Recent progress of catalysts for photocatalytic and photo(electro)catalytic NNR

The hydrogenation from N_2 to NH_3 is a reaction of exothermic and entropy reduction [78] (Eqn. (8)), so the experimental conditions of low temperature and high pressure are more conducive to improve NH_3 yield. However, the kinetics of the reaction is severely limited due to the high bond energy and stability of the N≡N triple bond. Fig. 5 shows the development of heterogeneous NRR catalysts in detail. Haber-Bosch reaction with high energy density based on Fe catalysts established in the early 19th century provided the possibility for artificial nitrogen fixation under high temperature and high pressure conditions at the cost of energy consumption and environmental pollution. Since then, the advanced Kellogg NH_3 synthesis process (KAAP) with metal Ru as the cocatalyst of NRR reaction jointly developed by British Petroleum and Kellogg Company of the United States in 1992 greatly promoted the large-scale production of NH_3 in industry. Although the addition of metal Ru increased the experimental cost, it achieved a new breakthrough in artificial nitrogen fixation under low temperature and low pressure for the first time. Subsequently, people continually study the NRR to seek new opportunities for artificial nitrogen fixation under normal temperature and pressure conditions. So far, the third generation new NRR catalysts, including BiOI [80], Ni_2P/$Cd_{0.5}Zn_{0.5}S$ [81], SnO_2/MoS_2 [82], Ag-Au@ZIF [83], etc., are developing vigorously to achieve new breakthrough of NH_3 synthesis process.

$$N_2 + 3H_2 \rightarrow 2NH_3 \quad \Delta H^{\theta} = -92.22\ kJ \cdot mol^{-1}$$
$$\Delta S^{\theta} = -92\ J \cdot mol^{-1} \cdot K^{-1} \tag{8}$$

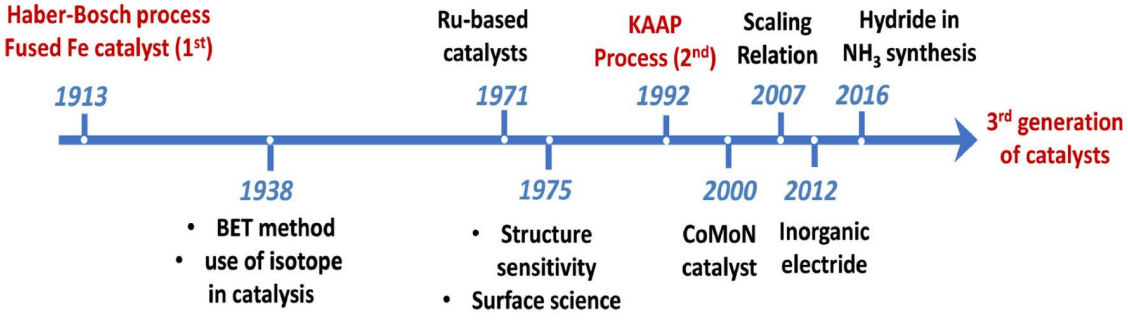

Fig. 5. Some progress in the development of NH_3 synthesis catalysis [79].

4.1. Defect engineering

Defect engineering is an effective strategy to regulate the electronic structure and chemical properties of materials, and is used in designing advanced catalysts. In solid surface chemistry, according to the size of defect, defect engineering is divided into the following four types: point defect, line defect, surface defect and volume defect [84]. In catalysis field, different defect states are selected in the light of the different reaction requirements.

As a non-toxic and environmentally friendly semiconductor material, TiO_2 is often used in various photocatalytic reactions due to its stable physical and chemical properties, suitable energy band structure. However, its photocatalytic performance is still unsatisfactory owing to its large band gap, high photogenerated carrier recombination rate and low reactive active site [85]. Introducing vacancy sites into TiO_2 through structural modification engineering can effectively solve the above problems and further broaden its universality and catalytic activity. There are three reasons: (1) The vacancy can be used as electron trapping centers to capture photogenerated electrons or holes, which avoids the recombination of photogenerated carriers and prolongs their life; (2) The vacancy can also be used as surface active sites to promote the adsorption and activation of reactive species on the catalyst surface; (3) The vacancy can also effectively narrow the band gap of semiconductors to enhance light absorption. However, inherent vacancy may not be "all good" in the strict sense. Recent studies indicate that only vacancy on the surface can enhance the photocatalytic activity. On the contrary, the vacancy in bulk phase can promote the recombination of photogenerated carriers, thereby reducing the photocatalytic efficiency. Perng et al. prepared amorphous TiO_2 films containing oxygen vacancy using atomic layer deposition technology [86]. After 100 amorphous deposition cycles, oxygen vacancy are changed from surface vacancy to bulk vacancy, which leads to the decrease of photocurrent and the increase of photogenerated carrier recombination rate. The conduct band and valence band of the photocatalyst are close to each other due to introduction of vacancy state levels, which reduces the band gap energy and weakens the oxidation/reduction capability of the semiconductor [87]. In addition, the photogenerated electrons will also undergo vibrational relaxation in the vacancy state energy level and thus become inactive. Only the electrons that absorb the high photon energy and overcome the vacancy level can effectively activate N_2. Up to now, various physical/chemical methods have been developed and applied to vacancy construction, such as high temperature annealing in an inert atmosphere, chemical reduction, vacuum activation, ultraviolet irradiation, plasma etching and rapid heating phase transformation [88].

4.1.1. Oxygen vacancy

As a typical anionic vacancy, oxygen vacancy often exist in metal oxide semiconductors. Zhang et al. prepared BiOBr nanosheets containing oxygen vacancy (BOB-001-OV) by a simple solvothermal method for photocatalytic synthesis of NH_3 [89]. The NH_3 yield is as high as 104.2 $\mu mol \cdot h^{-1} \cdot g^{-1}$ and 223.3 $\mu mol \cdot h^{-1} \cdot g^{-1}$ under visible light and full spectrum, respectively, without any sacrificial agent or noble metal cocatalyst. Theoretical calculation results show that when N_2 molecule and two Bi atoms with unsaturated coordination around N_2 molecule are loaded on the (001) crystal plane of BOB-001-OV by the end-bonding model, the delocalized free electrons are transferred from the oxygen vacancy level to the π antibonding orbital of N_2, and the bond length of N-N bond is increased from 1.078 Å to 1.133 Å. The adsorption and activation of N_2 are effectively realized. The oxygen vacancy also promote the separation of photogenerated carrier and the transfer of interfacial charge, which significantly enhances the light absorption of the sample and improves the photocatalytic efficiency. The change of catalyst surface functional groups during NRR was recorded by *in situ* diffuse reflection Fourier transform infrared spectroscopy. Compared with the complete BOB-001-H crystal, the N—H bond stretching vibration at 3550 cm^{-1}, the N—H bond bending vibration at 1711 cm^{-1} and 1557 cm^{-1} can be identified for BOB-001-OV sample with inherent vacancy. In addition, the vibration peaks at 2870 cm^{-1} and 1415 cm^{-1} attributed to adsorption of NH^{4+} ions further verified the positive effect of oxygen vacancy on NRR activity. However, during the photocatalytic nitrogen fixation reaction, the oxygen vacancy on the surface of BiOBr are easily occupied by O atoms in H_2O molecules, resulting in the reduction of catalytic active sites and the decrease of nitrogen fixation efficiency. Hence, cycle stability has become an important factor to limit the practical application of photocatalytic semiconductors with inherent vacancy. Subsequently, Chen et al. reported that oxygen vacancies formed in Bi_5O_7Br nanotubes via light induction effectively solved the problem of photocatalytic nitrogen fixation stability of bismuth oxide halide semiconductors [90]. The main photocatalytic process can be summarized as the following three steps. First, oxygen

atoms are detached from the surface of Bi_5O_7Br nanotubes under light, OER reaction occurs and oxygen vacancy are generated. Then, N_2 molecules are adsorbed and activated at the surface vacancy sites, and participate in the subsequent reduction reaction together with protons and electrons. Finally, when the NH_3 molecules are desorbed from the surface, the O atoms in H_2O occupy the oxygen vacancies, and the Bi_5O_7Br nanotubes are recovered. The high O content in Bi_5O_7Br and oxygen vacancy make Bi_5O_7Br nanotubes show higher photocatalytic activity and stability than BiOBr. The visible light photocatalytic NH_3 yield is as high as 1.38 $mmol \cdot h^{-1} \cdot g^{-1}$ at 420 nm, which is 12.5 times higher than that of BiOBr, and apparent quantum yield is over 2.3%. Zhao et al. loaded Pt nanoparticles on the surface of oxygen-enriched $NaNbO_3$ with a combination of ion exchange and light deposition [91]. The introduced oxygen vacancies increased the Fermi level and lowered the work function, thereby accelerating the transfer and separation of photogenerated charges. The oxygen vacancies also promoted the adsorption and activation of N_2. The Pt/O-$NaNbO_3$ exhibited high photocatalytic NRR efficiency under simulated solar light. Our research group deposited V_o-BiOBr on the surface of anodized TiO_2 nanotube arrays using ultrasonic assisted electrophoretic deposition for photoelectrocatalytic nitrogen fixation (Fig. 6a) [92]. The constructed V_o-BiOBr/TiO_2 nanotube arrays exhibited significantly higher NH_3 yield than BiOBr/TiO_2 (Fig. 6b). The heterojunction between V_o-BiOBr and TiO_2 not only enhances the light absorption, but also inhibits the recombination of photogenerated carriers. In addition, the introduction of V_o enhances the Lewis basicity of N_2 molecules by trapping photogenerated electrons in the conduction band and transferring them to N_2 adsorbed on the surface, which creates favourable conditions for the subsequent hydrogenation reduction.

Recently, Shiraishi et al. studied on the catalytic reaction mechanism of N_2 at the vacancy of commercial rutile TiO_2 semiconductor [43]. Taking the (110) crystal plane of rutile TiO_2 as an example, the O-bridge growing in the direction of (001) produces two Ti^{3+} ions by transferring two delocalized electrons to the 3d orbitals of near Ti^{4+} ions. Since the impurity state introduced by generating Ti^{3+} ions is lower than the conduction band of TiO_2, it can be used as the trapping center of photogenerated electrons, thus enhancing the photocatalytic activity of N_2. Electron paramagnetic spin resonance (EPR) spectroscopy confirmed the existence of bridging oxygen (O_b) vacancies in TiO_2 catalyst. After adding N_2, the ESR signal disappeared, indicating that the electrons are transferred from Ti^{3+} ions to adsorbed N_2 molecules. Accordingly, oxygen vacancies in TiO_2 played the key role in the photocatalytic NRR.

4.1.2. Nitrogen vacancy

The adsorption and activation of N_2 by oxygen vacancy and the high NRR catalytic performance from enhanced interfacial charge transfer induce the exploration and research of nitrogen vacancy in materials. The well-matched shape and size between nitrogen vacancy and N_2 molecules make nitrogen vacancy an important candidate for constructing NRR active sites. As a common semiconductor material, g-C_3N_4 has been widely used in different kinds of photocatalytic reactions [93−96], and structural control engineering has been developed to enhance its catalytic performance [97−101]. Zhang et al. introduced nitrogen vacancies in g-C_3N_4 nanosheet photocatalyst by annealing g-C_3N_4 in N_2 atmosphere at high temperature [30], which not only realized the selective adsorption and activation of N_2 molecules, but also promoted the separation of photogenerated carriers and the transfer of electrons to N_2. As a result, the photocatalytic NRR performance was

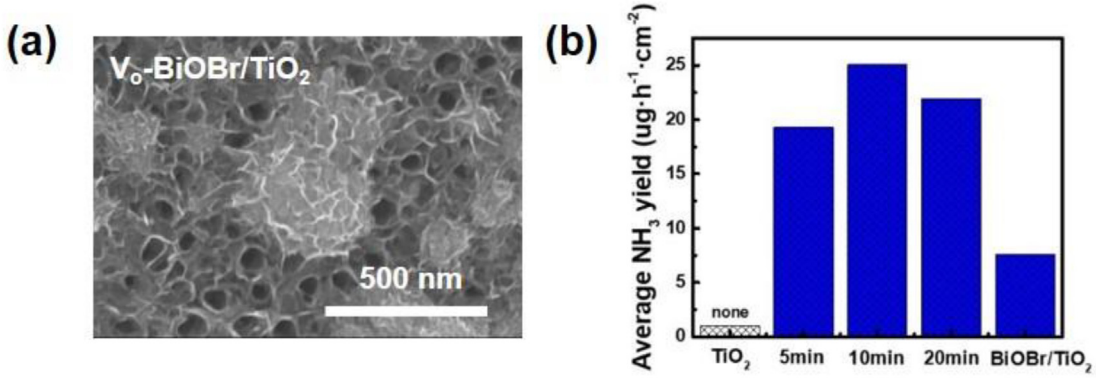

Fig. 6. (a) SEM image of V_o-BiOBr/TiO_2 nanotube arrays; (b) The average NH_3 yield plot of TiO_2, BiOBr/TiO_2 and V_o-BiOBr/TiO_2 with different deposition time [92].

significantly improved and the photocatalytic nitrogen fixation using air as the N source under environmental conditions was realized. Similarly, Dong et al. also synthesized the g-C_3N_4 nanosheets without and containing nitrogen vacancy (V-g-C_3N_4) by annealing monomelamine first at 500 °C in an air and then at 520 °C in N_2 atmosphere, respectively [20]. The specific surface area of V-g-C_3N_4 is twice that of g-C_3N_4, the adsorbed N_2 molecule content on the surface is as high as 75.1 $m^3 \cdot g^{-1}$, and the NH_3 yield is 1.24 $mmol \cdot h^{-1} \cdot g^{-1}$, indicating that the introduction of nitrogen vacancy increases the photocatalytic nitrogen fixation efficiency.

In addition, nitrogen vacancy is also applied to electrocatalytic nitrogen fixation because it can regulate the energy band and electronic structure of nanomaterials. Recent studies show that transition metal nitrides, such as VN, CrN, ZrN and NbN, have low NRR overpotential [56,102−104]. Yu et al. introduced nitrogen vacancy (NV) into metal-free polymeric carbon nitride (PCN) by annealing PCN at high temperature in the inert atmosphere of Ar gas to achieve efficient electrocatalytic NRR [105]. The nitrogen content in PCN was tuned by controlling the reaction time. Compared with PCN, the XRD pattern of PCN-NV reveals a narrow diffraction peak with lower intensity, which suggests that PCN-NV contains rich coordination unsaturated structures. The UV-Vis diffuse reflectance spectra confirm that the introduction of nitrogen vacancy promotes the delocalization of π electrons in the conjugated system. The light absorption is enhanced. The theoretical calculation data show that when N_2 molecule is adsorbed on PCN-NV through the end-bonding model, electrons are transferred from the C atom around the nitrogen vacancy to the adsorbed N_2 molecule, the bond length of the N≡N triple bond is increased, and thus N_2 molecules are effectively activated. PCN-NV exhibited excellent electrocatalytic NRR activity compared with PCN, having the NH_3 yield and Faradaic efficiency of 8.09 $\mu g \cdot h^{-1} \cdot mg^{-1}$ and 11.59 %, respectively. The cycle test further confirmed the good electrocatalytic NRR stability of PCN-NV, which is conducive to long-term service.

4.1.3. Sulfur vacancy

Inspired by biological nitrogen fixation in nature, Mo- and S-based nanomaterials are also considered as ideal catalysts with high NRR activity [106−110]. Recently, Sun et al. first calculated the electrochemical NRR processes at different sites on the surface of MoS_2 [111]. The Mo edge with positively charge is the activation site for N_2 molecular polarization. The transfer of electrons occurs from the N_2 molecule to the Mo atom on the edge. While the N−Mo bond is formed, the N≡N triple bond is weakened. Accordingly, MoS_2 with more edge sites will have higher NRR activity. Subsequently, MoS_2 nanosheet arrays grown vertically on a carbon-cloth substrate were prepared for electrocatalytic synthesis of NH_3. The NH_3 yield and Faradaic efficiency reached 8.08×10^{-11} $mol \cdot s^{-1} \cdot cm^{-2}$ and 1.17%, respectively, which is ascribed to the vertical structure exposing more marginal sites. Furthermore, the MoS_2 nanosheets showed good electrocatalytic nitrogen fixation activity even in an acidic solution. This provides a new idea for designing transition metal sulfides for efficiently catalytic NRR under environmental conditions.

Sulfur vacancy have also aroused great interest in regulating the electronic structure of nanomaterials and catalytic NRR due to the electronic structure and chemical property of S element similar to those of O element in the main group. Xia et al. introduced sulfur vacancy in a heterostructured $BiVO_4$/$ZnIn_2S_4$ for photocatalytic nitrogen fixation under visible light [112]. The introduced sulfur vacancy not only serves as the surface active site for N_2 adsorption and activation, but also can trap photogenerated electrons and change the local electronic structure on heterojunction surface, thus promoting the transfer of interfacial charge from the catalyst to N_2 molecules. The NRR activity was significantly enhanced. Recently, Zhang et al. prepared ultra-thin MoS_2 nanosheets through ultrasonically treating MoS_2 nanosheets in water for different time [42]. The ultra-thin nanosheet structure and ultrasonic treatment provide convenient conditions for the introduction of sulfur vacancy. The results of ICP test show that the stoichiometric ratio of Mo:S is 1:1.75, which is much lower than the theoretical 1:2, which confirms the existence of sulfur vacancy in MoS_2 nanoflakes. The photocatalytic nitrogen fixation experiments further show that the MoS_2 nanosheets with sulfur vacancy have higher nitrogen fixation activity than commercial or pristine MoS_2 nanosheets, and the NH_3 yield is 325 $\mu mol \cdot g^{-1} \cdot h^{-1}$.

In summary, anion (O, N, S) vacancies can effectively regulate the electronic structure and band gap of nanomaterials, and increase active sites on the semiconductor surface and further enhance the catalytic NRR activity. However, there are few studies on cationic vacancy in NRR. It is believed that the design of highly efficient nitrogen fixation catalysts that induce cationic vacancy will become another research focus in the field of NRR in the near future, and together with the influence

of anion vacancy, explain the positive role of inherent vacancy in NRR.

4.2. Atomic doping

In addition to ion vacancy, doping atom is also considered to be an effective way to control the surface properties of materials. Doping metallic or nonmetallic elements into metallic or nonmetallic compounds can effectively change their chemical properties such as elemental valence and atomic coordination number. Various types of catalytic reactions, such as oxidation reduction reaction (ORR) [113], CO_2 reduction reaction (CRR) [114] and OER [115], have demonstrated the positive effect of atom doping on catalyst reactivity. If more surface active sites can be introduced into the catalyst through doping atoms, the significantly enhanced NRR performance is expected.

4.2.1. Metal doping

As mentioned above, the impurity state levels in a material can be created through introduction of external atoms into the host lattice to improve the overall catalytic performance. In both photocatalysis and electrocatalysis, the purpose of doping heterogeneous atoms is to promote the adsorption and activation of N_2. However, except a few transition metals, most doped metals are not suitable for the NH_3 synthesis reaction because they cannot form strong bonds with N_2. Norskov et al. studied the NRR process of different metal surfaces and constructed a volcanic curve [116]. The results show that only Mo, Fe, Rh and Ru can effectively reduce N_2. The transition metal transfers unpaired electrons from the d orbital to the π antibonding orbital of N_2 to form a covalent bond, effectively weakening the N≡N triple bond. As an impurity species that can effectively activate N_2 molecules, Fe ion is widely used in the doping of semiconductor materials such as TiO_2 [117], g-C_3N_4 [118] and graphene [119]. Recently, Fe^{3+}-doped g-C_3N_4 was used for photocatalysis NRR to synthesize NH_3. When the N_2 molecule is adsorbed on the surface of Fe^{3+}, the delocalized electrons in the σ_g 2p orbital (HOMO) of the N_2 molecule overlap with the π_g* 2p orbital (LUMO), which increases the length of the N−N bond from 1157 Å to 1181 Å, and thus achieves effective activation of the N_2 molecule. Besides, Fe^{3+} can also be used as the capture center of photogenerated electrons, avoiding the recombination of photogenerated carriers. When the doping concentration of Fe^{3+} ion is 0.05wt%, the NH_3 yield of Fe^{3+}-doped g-C_3N_4 is 5.4 $mg \cdot L^{-1} \cdot h^{-1} \cdot g^{-1}$, which is about 13.5 times that of pure g-C_3N_4 [120]. Gao et al. doped metal element Mo in ultra-fine $W_{18}O_{49}$ nanowires to induce oxygen vacancy and form Mo−W bimetallic active sites for N_2 activation [121]. On the one hand, the doped metal Mo forms impurity state levels in the $W_{18}O_{49}$ bandgap so that the energy released by the photogenerated electrons in the relaxation process can be retained for photocatalytic NRR. On the other hand, the doped metal Mo replaces the complex-unsaturated W^{5+} ions in $W_{18}O_{49}$ nanowires due to the presence of oxygen vacancy, which increases the covalency of W−O bonds and promotes the transfer of electrons from Mo−W bonds to adsorbed N_2 molecules. Because the doping of metal Mo improves the local vacancy state in $W_{18}O_{49}$ nanowires and produces a multi-synergistic effect of N_2 activation, Mo-doped $W_{18}O_{49}$ nanowires show excellent catalytic performance in photocatalytic NRR. The apparent quantum yield at 400 nm is 0.33%, and the conversion efficiency of solar energy to NH_3 energy is 0.028%. He et al. doped Cu into Bi_2MoO_6 by a simple solvothermal method to replace Bi^{3+} with Cu^{2+} for photocatalytic nitrogen fixation [122]. Cu doping reduces the work function and increases the charge separation efficiency. Similarly, Bi-doped $CdMoO_4$ photocatalysts were also prepared using the same method [123]. Bi doping greatly decreases the particle size of $CdMoO_4$, boosts the activation of N_2 on Mo sites and improves the band structure of $CdMoO_4$, which facilitates photocatalytic NRR.

4.2.2. Nonmetallic doping

In addition to metal doping, non-metallic doping is also commonly used in various catalytic reactions. The charges are redistributed in the catalyst due to the differences in atomic size and electronegativity between the doped nonmetallic atoms and the adjacent C atoms. The adsorption of inert gases such as O_2 and CO_2 is strengthened. Therefore, the carbon-based nanomaterials doped with B, N, P and S show excellent catalytic performance in various heterogeneous reactions such as ORR and CRR [124]. It can be concluded from this that the ideal non-metallic doping nanomaterials should also be able to achieve the adsorption and deionization of N_2, and realize the catalytic NRR under environmental conditions. Non-metallic element B with unpaired electrons and empty orbitals has been used in designing nitrogen-fixing electrocatalysts because of its "electron accept-feedback" effect similar to that of transition metal elements. Ye et al. presented a new strategy for tailoring Bi bits of cathode by using B doping and rolling curvature [125]. The B doping in Bi matrix greatly reduces the energy

barrier of N_2 ->*NNH set step in NRR, while high curvature surface on the nanocoil is conducive to the adsorption of N_2. The integration of B doping and rolling curvature in a single cathode catalyst improve photoelectrocatalytic NRR performance when combined with a TiO_2 nanorod array as a photoanode to collect light and provide photogenerated electrons. The NH_3 yield is 29.2 $mg \cdot g^{-1} \cdot h^{-1}$, and the Faradaic efficiency is 8.3% at −0.48 V. Zheng et al. used B-doped graphene for electrocatalytic NRR [126]. On the one hand, the introduction of B atoms as an ideal Lewis acid site promotes the adsorption of N_2 and the formation of B−N active centers. On the other hand, the electron-deficient B atoms avoid the bonding of the catalyst with H^+ ions in water, and the Faradaic efficiency of the NRR reaction is increased. The highest NH_3 yield and Faradaic efficiency at −0.5 V are 9.8 $\mu g \cdot mg^{-1} \cdot h^{-1}$ and 10.8%, respectively, which are much higher than those of the undoped raw graphene. Since then, the B/N co-doped graphene [127] and O/S co-doped g-C_3N_4 [128] were also synthesized for electrocatalysis and photocatalytic nitrogen fixation, respectively.

4.3. Cocatalyst

Cocatalyst is a class of substances that is not active in itself, but can be coupled with the catalyst to change its electronic structure, grain size, ion valence and other physical and chemical properties so that improve the catalytic activity, reaction selectivity and cycle stability. In general, the cocatalyst can be divided into three different types, that is, reductive cocatalyst, oxidation cocatalyst and plasmon cocatalyst. The cocatalyst mainly plays the following roles in improving the photocatalytic or electrocatalytic reaction performance [129]: (1) Reducing the activation energy or overpotential of the redox half-reaction; (2) Promoting the separation of photogenerated electron-hole and avoiding the recombination of photogenerated carriers; (3) Inhibiting the photocorrosion of the material and improving its catalytic stability. Loading cocatalysts on semiconductor materials has been widely used in the photocatalytic hydrogen production by water splitting and the electrocatalytic CO_2 reduction. As stated above, HER and NH_3 synthesis reactions are a pair of competitive reactions in NRR process, and the generation of H_2 will greatly reduce the nitrogen fixation efficiency of the catalyst. Therefore, cocatalysts with good bonding ability for N_2 should be selected in NRR experiments, and the active catalysts such as Pt [130] and Pd [131] for HER reaction should be avoided.

4.3.1. Reduced cocatalyst

In view of the competition between HER reactions and NRR reactions, many researchers have devoted to develop non-precious metal or non-metallic cocatalysts to replace the traditional metal cocatalysts [132−134]. Transition metal phosphide with controllable electronic structure, changeable constituent elements and good electrical conductivity has attracted much attention. Fan et al. prepared $Cd_{0.5}Zn_{0.5}S$ loaded by NiP cocatalyst for photocatalytic nitrogen fixation [80]. The NiP promoted the separation of photogenerated carriers, and the apparent quantum yield at 420 nm was as high as 4.23%, and the NH_3 yield was 101.5 $\mu mol \cdot L^{-1} \cdot h^{-1}$, which is 35.7 times that of the unloaded NiP. Recently, black phosphorus (BP)-modified g-C_3N_4 nanosheets were proved to have excellent photocatalytic nitrogen fixation activity under visible light [135]. Since the C−P bond is formed on the catalyst surface, the electrons are closer to the P atom end, and thus the P atom can be used as an electron donor to transfer the photogenerated electrons to N_2 molecules adsorbed on the BP surface. After five cycles of photocatalytic nitrogen fixation experiments, the NH_3 yield of BP-modified g-C_3N_4 nanosheets did not decrease significantly, showing excellent catalytic stability.

In addition to the cocatalysts mentioned above, carbon-based nanomaterials are also considered to be a promising cocatalyst for photocatalytic nitrogen fixation. Liu et al. prepared a carbon quantum dot (CQDS) modified nitrogenase for biological nitrogen fixation [136]. The loading of CQDS accelerates the transfer of electrons between quantum dots and nitrogenase. The nitrogen fixation activity was 1.5 times higher than that of the free nitrogen fixation enzyme. Wang et al. also studied the effect of surface carbon modification on the photocatalytic nitrogen fixation reaction with $WO_3 \cdot H_2O$ hybrid as a catalyst [137]. The electrochemical impedance spectroscopic and photocurrent tests show that the modification of surface carbon promotes the separation of photogenerated carriers and the transfer of interfacial charge, and enhances the photocatalytic activity. The photocatalytic NH_3 evolution over P25, anatase TiO_2 and BiOBr can be significantly enhanced by decorating small amounts of carbon on their surface.

4.3.2. Plasmon type cocatalyst

Although metal Au is not an effective reducing cocatalyst for NRR, Au nanoparticles are often used in nitrogen fixation experiments due to local surface plasmon resonance (LSPR) effect [25,31,75,133,138]. The high-energy hot electrons generated by Au nanoparticles deposited on the

semiconductor surface can effectively overcome the Mott-Schottky barrier and transfer reversely to the conduction band of the semiconductor, and the photogenerated electrons and holes can be spatially separated between the semiconductor and the metal particles, and the optical properties of the sample was improved. However, when Au nanoparticles are loaded on the surface of pure catalyst alone for the synthesis of NH_3 reaction, the NH_3 nitrogen conversion efficiency is still unsatisfactory. Recently, TiO_2 with oxygen vacancy modified by Au nanoparticles, fabricated by Wang group [139] and Gong group [75], independently, showed excellent nitrogen fixation activity for photocatalytic and photoelectrocatalytic NRR. The oxygen vacancy promotes the adsorption and activation of N_2 molecules, while Au nanoparticles enhance the light absorption of the samples. Furthermore, both results display that the catalyst still has nitrogen fixation activity at 700 nm wavelength, which is impossible to pure TiO_2. In 2014, Misawa et al. served Nb-doped $SrTiO_3$ modified by Au nanoparticles as a catalyst and metal Ru as a cocatalyst for photoelectrochemical NRR [25]. Under illumination, the hot electrons produced by Au nanoparticles are first transferred to the conduction band of $SrTiO_3$, and then to the surface of Ru to participate in the reduction of N_2. However, different from the results of Ranjit et al. [54], although metal Ru can form a stable Had-Ru bond with adsorbed H for NRR, the HER with favorable kinetic significantly inhibits the generation of NH_3. Therefore, in 2016, Misawa et al. further replaced the metal Au with Zr/ZrO_x as the cocatalyst of NRR reaction [138]. The results show that Zr/ZrO_x can adsorb N_2 more easily than H atom, which improves the selectivity and NH_3 yield of the reaction. Based on the above analysis, even if Au nanoparticles can effectively improve the light absorption of the sample, it is still necessary to rely on structural modification engineering such as the introduction of vacancy, ion doping and cocatalyst to enhance nitrogen catalytic activity.

In addition to Au nanoparticles, other metals such as Ag, Cu, Ru and Pd can also achieve LSPR effect. Zhang et al. designed a photothermal catalytic system using TiO_2-xHx as a catalyst and Ru nanoparticles as a plasma cocatalyst for NRR [133]. The oxygen vacancy on the surface of TiO_2-xHx increases the electron state density around Ru nanoparticles and promotes the adsorption of N_2. The LSPR effect of Ru makes the local temperature of the catalyst surface up to 360 °C, and facilitates the activation and dissociation of N_2. TiO_2-xHx can reversibly receive H atoms from Ru surface adsorption and feed back to Ru nanoparticles for the hydrogenation reduction of N_2. This reaction system effectively avoids the toxic effect of H_2 on the catalyst, and thus achieves a stable and efficient ammonia-nitrogen conversion.

4.4. Heterojunction engineering

Heterojunction mainly refers to the interface formed by the contact between two kinds of semiconductors with different band structures, and is an important means to accelerate the photogenerated carrier separation and improve the photoelectrocatalytic performance. In general, the difference in energy band level between two semiconductors determines the heterojunction architectures and the flow direction of the photogenerated carriers, which can guide the catalytic reaction. At present, there are three main types of heterojunction architectures (Fig. 7).

When the band structure of two semiconductors is an inclusion relationship (Type I), the photogenerated carriers produced by the semiconductor A are transferred to the semiconductor B, and recombined on the semiconductor B, which is not

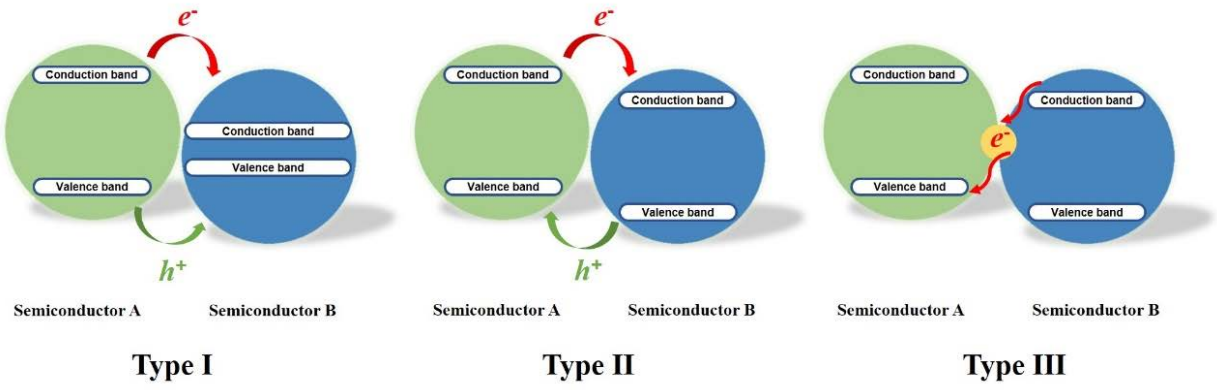

Fig. 7. Three common energy band structures in heterojunction [140].

conducive to the photo(electro)catalytic reaction. When the band structure of two semiconductors is staggered (Type II), the photogenerated electrons are transferred from the conduction band of the semiconductor A to that of the semiconductor B, while the photogenerated holes are transferred from the valence band of the semiconductor B to that of the semiconductor A. The spatial separation of photogenerated carriers effectively enhances photocatalytic activity [140]. Recently, Bharath et al. constructed layered Au-WS_2@RGOs hybrid heterojunctions with multiple electroactive sites by a simple hydrothermal and ion regulation method for photocatalytic nitrogen fixation under visible light irradiation [141]. It is found that the strong electron coupling in Au-WS_2@RGOs heterojunction photocatalyst promotes the separation of photogenerated carriers. At the same time, a unique porous network configuration of WS_2@RGOs provides a large active surface area to trap more N_2 molecules. The synergistic effect of Au and WS_2@RGOs improves the charge transfer, promotes the transfer of interfacial charge from the catalyst to N_2 molecules, and accelerates the NRR kinetics. Following the electron transfer mechanism of Type II, the NH_3 yield reaches 34 $\mu mol \cdot h^{-1} \cdot cm^{-2}$ and the FE is up to 16.2 % at −0.6 V. Our group constructed V_o-TiO_2/Ag@TiO_2 composite photocathode by depositing V_o-TiO_2 nanosheets and Ag nanoparticles on the surface of TiO_2 nanorods arrays successively by a pulsed electrodeposition and secondary solvothermal method [142]. The photoelectrocatalytic nitrogen fixation test showed that the NH_3 yield of V_o-TiO_2/Ag@TiO_2 was significantly higher than that of Ag@TiO_2 and TiO_2 (Fig. 8a). The three-dimensional structure of nanosheet-dot-rod not only enhances the ohmic contact of the interface, but also provides a good route for the transfer of photogenerated carriers (Fig. 8b). The LSPR effect of Ag nanoparticles and the heterojunction between different crystal phases of TiO_2 significantly improved the visible light response and carrier separation rate. The introduction of V_o enhanced the adsorption and activation of N_2 on the surface, and accelerated the interfacial charge transfer.

Type III is the same as Type II expect for the slightly difference of the transfer path of photogenerated carriers. Under light irradiation, the photogenerated electrons in the conduction band of the semiconductor B recombine with the photogenerated holes in the valence band of the semiconductor A, thus reducing the recombination rate of photogenerated carriers in the bulk phase. Because the direction of the electron shows a "Z" shape, it is also vividly called "Z-scheme" configuration [143]. Compared with Type II, the photogenerated electrons with a more negative reduction potential and the photogenerated holes with a more positive oxidation potential are retained on the surface of the original semiconductor, the "Z-scheme" system has excellent redox ability for photo(electro)catalytic reactions [8]. In 2017, Chen et al. coupled g-C_3N_4 with 3, 4-dihydroxybenzaldehyde functional group as an electronic intermediate to Ga_2O_3 for artificial NRR [144]. This is for the first time to use Z-scheme for nitrogen fixation, signifying a new breakthrough. The introduction of the aromatic ring enhances the ohmic contact of two semiconductors and acts as an electron transfer intermediate to promote the recombination of the photogenerated electrons of Ga_2O_3 with the photogenerated holes of g-C_3N_4. The photogenerated holes on the valence band of Ga_2O_3 oxidize OH^- to produce ·OH radical, and the photogenerated electrons on the conduction

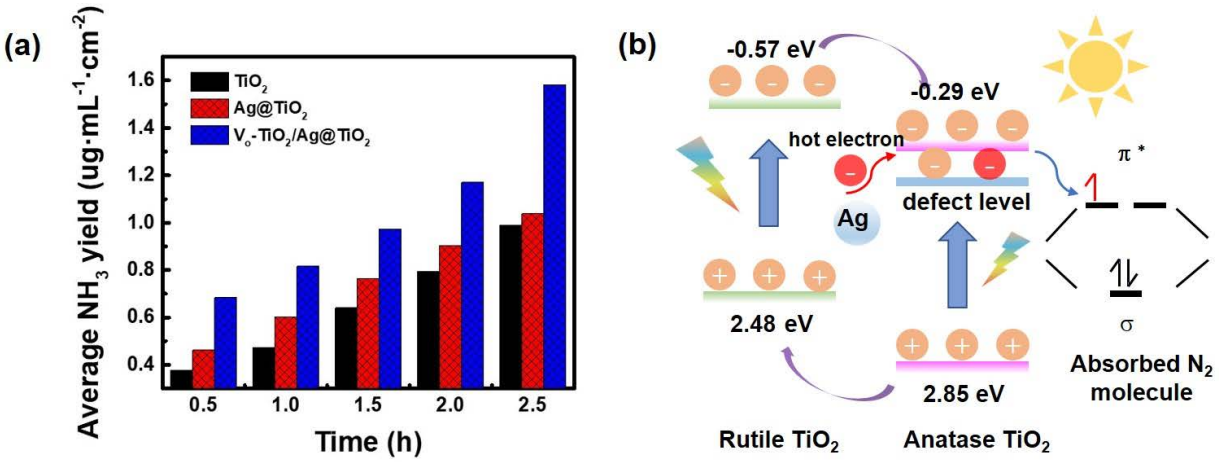

Fig. 8. (a) The average NH_3 yield plots of TiO_2, Ag@TiO_2 and V_o-TiO_2/Ag@TiO_2; (b) Proposed mechanism for photoelectrocatalytic nitrogen reduction over V_o-TiO_2/Ag@TiO_2 [142].

band of g-C_3N_4 reduce O_2 to produce H_2O_2 that is then decomposed into ·OH radical. The methanol as a sacrificial agent consumes ·OH free radical and promotes the production of NH_3. He et al. designed and synthesized a novel ternary composite photocatalyst by a solvothermal method [145]. The incorporation of Bi—Bi_2O_3 can transform $CdWO_4$ crystals into nanoparticles. The increased specific surface area improves the catalytic performance and thus the light absorption is greatly enhanced. The Bi metal, as a bridge that tightly binds $CdWO_4$ and Bi_2O_3, promotes the migration and separation of photogenerated charges. The Bi—Bi_2O_3/$CdWO_4$ composite presents higher photocatalytic nitrogen fixation performance. Hence, heterojunction engineering coupled by semiconductor has also become a feasible method to improve the NRR efficiency in the field of photocatalytic nitrogen fixation.

5. Mechanism of photoelectrocatalytic nitrogen fixation reaction

N_2 is one of the few inert gases in the world, and the first hydrogenation of N_2 molecule is considered to be the rate determined step in the NRR reaction process. A large amount of energy is required to activate the N≡N triple bond to decompose N_2 molecule. Up to now, reducing N_2 to NH_3 on the surface of heterogeneous catalysts mainly follows two reaction mechanisms: the dissociation mechanism and the association mechanism. A schematic diagram of NRR mechanism is illustrated in Fig. 9a [146]. According to the dissociation mechanism, N_2 molecules adsorbed on the catalyst surface are first dissociated to generate two independent N atoms by breaking the N≡N triple bond. The two N atoms are then respectively hydrogenated with H atoms to produce NH_3. Because the dissociation of N_2 requires an extremely large amount of energy, the traditional industrial Haber-Bosch NH_3 production process often follows this mechanism. On the contrary, photocatalyzed, electrocatalyzed or photoelectrocatalyzed NRR under mild conditions follow the association mechanism. In the association mechanism, after N_2 molecules receive one proton and one electron from the surrounding environment to produce chemisorbed species, different reaction intermediates can be formed through the distal association mechanism and the alternate association mechanism. In the distal association mechanism, the distal N atom first undergoes the continuous hydrogenation in which the protons combine with the electrons. The hydrogenation reduction of the proximal N atom takes place after the resulting NH_3 molecules are detached from the catalyst surface. In the selective association mechanism, the hydrogen reduction combining protons with electrons alternates between the two N atoms, and the NH_3 molecules formed are released successively. It is noteworthy that different from the dissociation mechanism, in the association mechanism, the two N atoms still maintain mutual bonding and are adsorbed on the surface of the catalyst together in the form of terminal contact. In addition to the above two conventional reaction mechanisms, the Mars-van Krevelen (MvK) reaction mechanism is proposed for the NRR process that occurs on the transition metal nitride surface, and its reaction route is shown in Fig. 9b. First, the N atom on the surface of the transition metal nitride is hydrogenated to NH_3 and nitrogen vacancy is formed. Subsequently, N_2

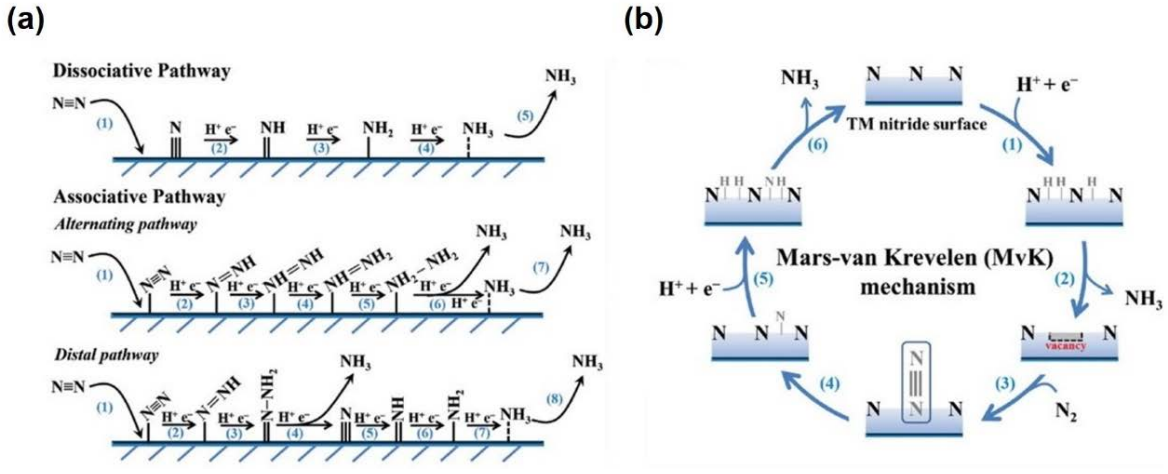

Fig. 9. Reaction mechanism diagrams of nitrogen reduction [146].

dissolved in the electrolyte is transferred to the solid surface to fill the nitrogen vacancy and maintain the catalyst to regenerate. Finally, the distal N atom in the N_2 molecule is hydrogenated to reduce, and a second NH_3 molecule is released to complete the catalytic cycle. The theoretical calculation proved that MvK reaction mechanism is more suitable for NRR process on transition metal nitride surface than dissociation mechanism and association mechanism [131].

On the whole, from the optimization of reaction conditions to the innovation of experimental equipments, from the construction of new catalysts to the deepening of reaction mechanisms, the understanding of NRR gradually deepens. The development process of artificial nitrogen fixing catalyst has also witnessed numerous researchers' assiduous exploration in scientific research.

6. Conclusions and outlooks

Over the past half-century, semiconductor photocatalysis technology has emerged as a forefront and pivotal branch in fundamental research. Achieving the maturity and industrialization of semiconductor photocatalysis technology holds paramount strategic importance in alleviating the energy crisis and curbing environmental pollution. Despite significant progress, certain key technical barriers and challenges persist, requiring further breakthrough. Systematic research efforts are essential, focusing on the following aspects.

At present, there is still no recognized constant standard for photo(electro)catalytic nitrogen fixation. Typically, the units evaluating the nitrogen fixation yield are different for photocatalysis ($\mu g \cdot mg^{-1} \cdot h^{-1}$), electrocatalysis ($mol \cdot s^{-1} \cdot cm^{-2}$) and photoelectrocatalysis ($\mu g \cdot cm^{-1} \cdot h^{-1}$), which calls for standardization in the future research and development.

At the same time, in the process of nitrogen fixation, it is difficult to compare the performance of different catalysts because the experimental conditions, including the optical power density, the composition, concentration and pH of electrolyte, and reaction time have no unified standards. Therefore, it is necessary to choose a more scientific computational tool to reasonably normalize different experimental conditions, such as apparent quantum yield (AQY).

Another factor that may affect the accurate determination of trace levels of NH_3 is the selectivity of the catalyst. The decomposition of NH_3 and the by-products of H_2 evolution should be avoided. Especially in the water phase reaction, the contents of hydrazine, nitrite and nitrate need to be detected. At the same time, in order to more accurately measure the nitrogen fixation yield, and effectively eliminate the possible NH_3 pollution in the air and the electrolyte, the characterization method of ^{15}N isotope is recommended in the study.

Since the photoelectrocatalytic reaction generally adopts the test method of splitting the REDOX reaction, that is, the photoanode and the photocathode are not in the same reaction chamber, the current reports on photoelectrocatalytic nitrogen fixation mostly focus on the photocathode where N_2 reduction reaction occurs, while few reports on the modification of the photoanode where H_2O oxidation occurs to improve the catalytic performance. The simultaneous optimization of the photoanode and photocathode with different catalysts for nitrogen fixation is worthy of expectation, which is a promising research route of photoelectrocatalytic nitrogen fixation.

The development of more advanced characterization methods and testing techniques, such as in-situ Raman spectroscopy, *in-situ* infrared spectroscopy, and *in-situ* ultrafast spectroscopy, is imperative for achieving profound breakthroughs in basic theoretical research. It is essential to further explore the separation, transfer and reaction paths of photogenerated carriers in semiconductor materials, along with an in-depth understanding of the mechanisms involved in the adsorption, intermediation and desorption of N_2 molecules in the photocatalytic nitrogen fixation process. *In-situ* Raman spectroscopy can detect the nitrogen reaction intermediates adsorbed on the catalyst surface, and better determine the reaction route of N_2 reduction during the catalytic process. By employing density functional theory (DFT), the band structure and surface state of semiconductor photocatalysts can be calculated and simulated on a computer. Time-resolved transient fluorescence spectroscopy is useful to study the kinetics of photogenerated carriers in semiconductor catalysis. These endeavors aim to provide robust theoretical support for the design and preparation of more efficient photocatalysts.

In the other aspects, enhancements are needed across the entire photocatalytic nitrogen fixation process, covering fundamental electrode design, the electrode production process, and the development of corresponding components to boost photocatalytic nitrogen fixation performance. Furthermore, there is a critical need for the design of a systematic and standardized photocatalytic nitrogen fixation system that simulates industrial production process. Such an approach renders advances in the industrial application of photocatalytic nitrogen fixation technology.

Acknowledgements

This work was financially supported by the Natural Science Foundation of Fujian Province of China (No. 2021J01021).

References

[1] Rao L, Xu X, Adamo C. Theoretical investigation on the role of the central carbon atom and close protein environment on the nitrogen reduction in Mo nitrogenase[J]. ACS Catal., 2016, 6(3): 1567−1577.

[2] Lai F, Zong W, He G, Xu Y, Huang H, Weng B, Rao D, Martens J A, Hofkens J, Parkin I P, Liu T. N_2 Electroreduction to NH_3 by selenium vacancy-rich $ReSe_2$ catalysis at an abrupt interface[J]. Angew. Chem. Int. Ed., 2020, 59(32): 13320−13327.

[3] Sim H YF, Chen J RT, Koh C SL, Lee H K, Han X, Phan-Quang G C, Pang J Y, Lay C L, Pedireddy S, Phang I Y, Yeow E KL, Ling X Y. ZIF-induced d-band modification in a bimetallic nanocatalyst: achieving over 44% efficiency in the ambient nitrogen reduction reaction[J]. Angew. Chem. Int. Ed., 2020, 59(39): 16997−17003.

[4] Hochman G, Goldman A S, Felder F A, Mayer J M, Miller A JM, Holland P L, Goldman L A, Manocha P, Song Z, Aleti S. Potential economic feasibility of direct electrochemical nitrogen reduction as a route to ammonia [J]. ACS Sustain. Chem. Eng., 2020, 8(24): 8938−8948.

[5] Wang Z Q, Li C J, Deng K, Xu Y, Xue H R, Li X N, Wang L, Wang H J. Ambient nitrogen reduction to ammonia electrocatalyzed by bimetallic PdRu porous nanostructures[J]. ACS Sustain. Chem. Eng., 2018, 7(2): 2400−2405.

[6] Kitano M, Inoue Y, Yamazaki Y, Hayashi F, Kanbara S, Matsuishi S, Yokoyama T, Kim S W, Hara M, Hosono H. Ammonia synthesis using a stable electride as an electron donor and reversible hydrogen store[J]. Nat. Chem., 2012, 4(11): 934−940.

[7] Suryanto B HR, Du H L, Wang D, Chen J, Simonov A N, Macfarlane D R. Challenges and prospects in the catalysis of electroreduction of nitrogen to ammonia[J]. Nat. Catal., 2019, 2(4): 290−296.

[8] Wang S C, Liu G, Wang L Z. Crystal facet engineering of photoelectrodes for photoelectrochemical water splitting [J]. Chem. Rev., 2019, 119(8): 5192−5247.

[9] Li S J, Bao D, Shi M M, Wulan B R, Yan J M, Jiang Q. Amorphizing of Au nanoparticles by CeO_x-RGO hybrid support towards highly efficient electrocatalyst for N_2 reduction under ambient conditions[J]. Adv. Mater., 2017, 29(33): 170001.

[10] Chu K, Cheng Y H, Li Q Q, Liu Y P, Tian Y. Fe-doping induced morphological changes, oxygen vacancies and Ce^{3+}-Ce^{3+} pairs in CeO_2 for promoting electrocatalytic nitrogen fixation[J]. J. Mater. Chem. A, 2020, 8(12): 5865−5873.

[11] Zhang R, Guo H R, Yang L, Wang Y, Niu Z G, Huang H, Chen H Y, Xia L, Li T S, Shi X F, Sun X P, Li B H, Liu Q. Electrocatalytic N_2 fixation over hollow VO_2 microspheres at ambient conditions[J]. Chemelectrochem, 2019, 6(4): 1014−1018.

[12] Guo C, Ran J, Vasileff A, Qiao S Z. Rational design of electrocatalysts and photo(electro)catalysts for nitrogen reduction to ammonia (NH_3) under ambient conditions[J]. Energy Environ. Sci., 2018, 11(1): 45−56.

[13] Kumar D, Pal S, Krishnamurty S. N_2 activation on Al metal clusters: catalyzing role of BN-doped graphene support[J]. Phys. Chem. Chem. Phys., 2016, 18(40): 27721−27727.

[14] Bezdek M J, Chirik P J. Expanding boundaries: N_2 cleavage and functionalization beyond early transition metals [J]. Angew. Chem. Int. Ed., 2016, 55(28): 7892−7896.

[15] Shipman M A, Symes M D. Recent progress towards the electrosynthesis of ammonia from sustainable resources [J]. Catal. Today, 2017, 286: 57−68.

[16] Morales-Guio C G, Stern L A, Hu X. Nanostructured hydrotreating catalysts for electrochemical hydrogen evolution[J]. Chem. Soc. Rev., 2014, 43(18): 6555−6569.

[17] Hu G, Hu C X, Zhu Z Y, Zhang L, Wang Q, Zhang H L. Construction of Au/CuO/Co_3O_4 tricomponent heterojunction nanotubes for enhanced photocatalytic oxygen evolution under visible light irradiation[J]. ACS Sustain. Chem. Eng., 2018, 6(7): 8801−8808.

[18] Sun Y, Sinev I, Ju W, Bergmann A, Dresp S, Kühl S, Spöri C, Schmies H, Wang H, Bernsmeier D, Paul B, Schmack R, Kraehnert R, Roldan Cuenya B, Strasser P. Efficient electrochemical hydrogen peroxide production from molecular oxygen on nitrogen-doped mesoporous carbon catalysts[J]. ACS Catal., 2018, 8(4): 2844−2856.

[19] Xu F Y, Meng K, Cheng B, Wang S Y, Xu J S, Yu J G. Unique S-scheme heterojunctions in self-assembled TiO_2/$CsPbBr_3$ hybrids for CO_2 photoreduction [J]. Nat. Commun., 2020, 11(1): 4613.

[20] Dong G H, Ho W K, Wang C Y. Selective photocatalytic N_2 fixation dependent on g-C_3N_4 induced by nitrogen vacancies[J]. J. Mater. Chem. A, 2015, 3(46): 23435−23441.

[21] Hirakawa H, Hashimoto M, Shiraishi Y, Hirai T. Photocatalytic conversion of nitrogen to ammonia with water on surface oxygen vacancies of titanium dioxide[J]. J. Am. Chem. Soc., 2017, 139(31): 10929−10936.

[22] Xiang X J, Wang Z, Shi X F, Fan M K, Sun X P. Ammonia synthesis from electrocatalytic N_2 reduction under ambient conditions by Fe_2O_3 nanorods[J]. Chemcatchem, 2018, 10(20): 4530−4535.

[23] Guo W H, Liang Z B, Zhao J L, Zhu B J, Cai K T, Zou R Q, Xu Q. Hierarchical cobalt phosphide hollow nanocages toward electrocatalytic ammonia synthesis under ambient pressure and room temperature[J]. Small Methods, 2018, 2(12): 1800204.

[24] Jang Y J, Lindberg A E, Lumley M A, Choi K S. Photoelectrochemical nitrogen reduction to ammonia on cupric and cuprous oxide photocathodes[J]. ACS Energy Lett., 2020, 5(6): 1834−1839.

[25] Oshikiri T, Ueno K, Misawa H. Plasmon-induced ammonia synthesis through nitrogen photofixation with visible light irradiation[J]. Angew. Chem. Int. Ed., 2014, 53(37): 9802−9805.

[26] Furube A, Asahi T, Masuhara H, Yamashita H, Anpo M. Charge carrier dynamics of standard TiO_2 catalysts revealed by femtosecond diffuse reflectance spectroscopy [J]. J. Phys. Chem. B, 1999, 103(16): 3120−3127.

[27] Alexander B D, Kulesza P J, Rutkowska I, Solarska R, Augustynski J. Metal oxide photoanodes for solar hydrogen production[J]. J. Mater. Chem., 2008, 18(20): 2298−2303.

[28] Bak T, Nowotny J, Rekas M, Sorrell C C. Photo-electrochemical hydrogen generation from water using solar energy. Materials-related aspects[J]. Int. J. Hydrogen Energy, 2002, 27(10): 991−1022.

[29] Medford A J, Hatzell M C. Photon-driven nitrogen fixation: current progress, thermodynamic considerations, and future outlook[J]. ACS Catal, 2017, 7(4): 2624−2643.

[30] Wang W K, Zhou H J, Liu Y Y, Zhang S B, Zhang Y X, Wang G Z, Zhang H M, Zhao H J. Formation of BNC coordination to stabilize the exposed active nitrogen atoms in g-C_3N_4 for dramatically enhanced photocatalytic

ammonia synthesis performance[J]. Small, 2020, 16(13): e1906880.

[31] Xiao C, Hu H, Zhang X, Macfarlane D R. Nanostructured gold/bismutite hybrid heterocatalysts for plasmon-enhanced photosynthesis of ammonia[J]. ACS Sustain. Chem. Eng., 2017, 5(11): 10858−10863.

[32] Di J, Xia J, Chisholm M F, Zhong J, Chen C, Cao X, Dong F, Chi Z, Chen H, Weng Y X, Xiong J, Yang S Z, Li H, Liu Z, Dai S. Defect-tailoring mediated electron-hole separation in single-unit-cell Bi_3O_4Br nanosheets for boosting photocatalytic hydrogen evolution and nitrogen fixation[J]. Adv. Mater., 2019, 31(28): e1807576.

[33] Zhao Y, Zhao Y, Waterhouse G IN, Zheng L, Cao X, Teng F, Wu L Z, Tung C H, O'hare D, Zhang T. Layered-double-hydroxide nanosheets as efficient visible-light-driven photocatalysts for dinitrogen fixation[J]. Adv. Mater., 2017, 29(42): 1703828.

[34] Zhao Y, Zhao Y, Shi R, Wang B, Waterhouse G IN, Wu L Z, Tung C H, Zhang T. Tuning oxygen vacancies in ultrathin TiO_2 nanosheets to boost photocatalytic nitrogen fixation up to 700 nm[J]. Adv. Mater., 2019, 31(16): e1806482.

[35] Zhao Y, Hoivik N, Wang K Y. Recent advance on engineering titanium dioxide nanotubes for photochemical and photoelectrochemical water splitting[J]. Nano Energy, 2016, 30: 728−744.

[36] Ghosh S, Kouame N A, Ramos L, Remita S, Dazzi A, Deniset-Besseau A, Beaunier P, Goubard F, Aubert P H, Remita H. Conducting polymer nanostructures for photocatalysis under visible light[J]. Nat. Mater., 2015, 14(5): 505−511.

[37] Yang J H, Wang D G, Han H X, Li C. Roles of cocatalysts in photocatalysis and photoelectrocatalysis[J]. Acc. Chem. Res., 2013, 46(8): 1900−1909.

[38] Liu S Z, Li D G, Sun H Q, Ang H M, Tade M O, Wang S B. Oxygen functional groups in graphitic carbon nitride for enhanced photocatalysis[J]. J. Colloid Interface Sci., 2016, 468: 176−182.

[39] Nguyen C C, Vu N N, Do T O. Recent advances in the development of sunlight-driven hollow structure photocatalysts and their applications[J]. J. Mater. Chem. A, 2015, 3(36): 18345−18359.

[40] Reza Gholipour M, Dinh C T, Beland F, Do T O. Nanocomposite heterojunctions as sunlight-driven photocatalysts for hydrogen production from water splitting[J]. Nanoscale, 2015, 7(18): 8187−8208.

[41] Yang H Y, Zhou Y M, Wang Y Y, Hu S C, Wang B B, Liao Q, Li H F, Bao J H, Ge G Y, Jia S K. Three-dimensional flower-like phosphorus-doped g-C_3N_4 with a high surface area for visible-light photocatalytic hydrogen evolution[J]. J. Mater. Chem. A, 2018, 6(34): 16485−16494.

[42] Xie S J, Zhang Q H, Liu G D, Wang Y. Photocatalytic and photoelectrocatalytic reduction of CO_2 using heterogeneous catalysts with controlled nanostructures[J]. Chem. Commun. (Camb.), 2016, 52(1): 35−59.

[43] Hirakawa H, Hashimoto M, Shiraishi Y, Hirai T. Photocatalytic conversion of nitrogen to ammonia with water on surface oxygen vacancies of titanium dioxide[J]. J. Am. Chem. Soc., 2017, 139(31): 10929−10936.

[44] Feng X W, Chen H, Jiang F, Wang X. Enhanced visible-light photocatalytic nitrogen fixation over semicrystalline graphitic carbon nitride: oxygen and sulfur co-doping for crystal and electronic structure modulation[J]. J. Colloid Interface Sci., 2018, 509: 298−306.

[45] Li H, Shang J, Shi J G, Zhao K, Zhang L Z. Facet-dependent solar ammonia synthesis of BiOCl nanosheets via a proton-assisted electron transfer pathway[J]. Nanoscale, 2016, 8(4): 1986−1993.

[46] Luo J Y, Bai X X, Li Q, Yu X, Li C Y, Wang Z N, Wu W W, Liang Y P, Zhao Z H, Liu H. Band structure engineering of bioinspired Fe doped $SrMoO_4$ for enhanced photocatalytic nitrogen reduction performance[J]. Nano Energy, 2019, 66: 104187.

[47] Hu S Z, Chen X, Li Q, Li F Y, Fan Z P, Wang H, Wang Y J, Zheng B H, Wu G. Fe^{3+} doping promoted N_2 photofixation ability of honeycombed graphitic carbon nitride: the experimental and density functional theory simulation analysis[J]. Appl. Catal. B: Environ., 2017, 201: 58−69.

[48] Saadatjou N, Jafari A, Sahebdelfar S. Ruthenium nanocatalysts for ammonia synthesis: a review[J]. Chem. Eng. Commun., 2014, 202(4): 420−448.

[49] Ling C Y, Niu X H, Li Q, Du A J, Wang J L. Metal-free single atom catalyst for N_2 fixation driven by visible light [J]. J. Am. Chem. Soc., 2018, 140(43): 14161−14168.

[50] Simpson F B, Burris R H. A nitrogen pressure of 50 atmospheres does not prevent evolution of hydrogen by nitrogenase[J]. Science, 1984, 224(4653): 1095.

[51] Indra A, Menezes P W, Kailasam K, Hollmann D, Schroder M, Thomas A, Bruckner A, Driess M. Nickel as a co-catalyst for photocatalytic hydrogen evolution on graphitic-carbon nitride (sg-CN): what is the nature of the active species?[J]. Chem. Commun. (Camb.), 2016, 52(1): 104−107.

[52] Wang D, Liu Z P, Yang W M. Revealing the size effect of platinum cocatalyst for photocatalytic hydrogen evolution on TiO_2 support: a DFT study[J]. ACS Catal, 2018, 8(8): 7270−7278.

[53] Kong C, Li Z, Lu G X. The dual functional roles of Ru as co-catalyst and stabilizer of dye for photocatalytic hydrogen evolution[J]. Int. J. Hydrogen Energy, 2015, 40(17): 5824−5830.

[54] Ranjit K T, Varadarajan T K, Viswanathan B. Photocatalytic reduction of dinitrogen to ammonia over noble-metal-loaded TiO_2[J]. J. Photochem. Photobiol. A: Chem., 1996, 96(1): 181−185.

[55] Abghoui Y, Garden A L, Howalt J G, Vegge T, Skúlason E. Electroreduction of N_2 to ammonia at ambient conditions on mononitrides of Zr, Nb, Cr, and V: a DFT guide for experiments[J]. ACS Catal, 2015, 6(2): 635−646.

[56] Shi A Y, Li H H, Yin S, Hou Z L, Rong J Y, Zhang J C, Wang Y H. Photocatalytic NH_3 versus H_2 evolution over g-C_3N_4/Cs_xWO_3: O_2 and methanol tipping the scale[J]. Appl. Catal. B: Environ., 2018, 235: 197−206.

[57] Lee J, Park H, Choi W. Selective Photocatalytic oxidation of NH_3 to N_2 on platinized TiO_2 in water[J]. Environ. Sci. Technol., 2002, 36(24): 5462−5468.

[58] Li R. Photocatalytic nitrogen fixation: an attractive approach for artificial photocatalysis[J]. Chin. J. Catal., 2018, 39(7): 1180−1188.

[59] Schrauzer G N, Guth T D. Photolysis of water and photoreduction of nitrogen on titanium dioxide[J]. J. Am. Chem. Soc., 1977, 99(22): 7189−7193.

[60] Li Y H, Chen X, Zhang M J, Zhu Y M, Ren W J, Mei Z W, Gu M, Pan F. Oxygen vacancy-rich MoO_{3-x} nanobelts for photocatalytic N_2 reduction to NH_3 in pure water[J]. Catal. Sci. Technol., 2019, 9(3): 803−810.

[61] Sun S M, Li X M, Wang W Z, Zhang L, Sun X. Photocatalytic robust solar energy reduction of dinitrogen to ammonia on ultrathin MoS_2[J]. Appl. Catal. B: Environ., 2017, 200: 323−329.

[62] Zhang G, Ji Q H, Zhang K, Chen Y, Li Z H, Liu H J, Li J H, Qu J H. Triggering surface oxygen vacancies on atomic layered molybdenum dioxide for a low energy consumption path toward nitrogen fixation[J]. Nano Energy, 2019, 59: 10−16.

[63] Xiao C L, Wang H P, Zhang L, Sun S M, Wang W Z. Enhanced photocatalytic nitrogen fixation on MoO_2/BiOCl composite[J]. Chemcatchem, 2019, 11(24): 6467−6472.

[64] Mou H Y, Wang J F, Yu D K, Zhang D L, Chen W J, Wang Y Q, Wang D B, Mu T C. Fabricating amorphous g-C_3N_4/ZrO_2 photocatalysts by one-step pyrolysis for solar-driven ambient ammonia synthesis[J]. ACS Appl. Mater. Interfaces, 2019, 11(47): 44360−44365.

[65] Ithisuphalap K, Zhang H G, Guo L, Yang Q G, Yang H P, Wu G. Photocatalysis and photoelectrocatalysis methods of nitrogen reduction for sustainable ammonia synthesis [J]. Small Methods, 2018, 3(6): 1800352.

[66] Van Tamelen E E, Akermark B. Electrolytic reduction of molecular nitrogen[J]. J. Am. Chem. Soc., 1968, 90(16): 4492−4493.

[67] Wang J, Chen S L, Li Z J, Li G K, Liu X. Recent advances in electrochemical synthesis of ammonia through nitrogen reduction under ambient conditions[J]. Chemelectrochem, 2020, 7(5): 1067−1079.

[68] Marnellos G, Stoukides M. Ammonia synthesis at atmospheric pressure[J]. Science, 1998, 282(5386): 98−100.

[69] Licht S, Cui B, Wang B, Li F F, Lau J, Liu S. Ammonia synthesis by N_2 and steam electrolysis in molten hydroxide suspensions of nanoscale Fe_2O_3[J]. Science, 2014, 345(6197): 637−640.

[70] Manjunatha R, Schechter A. Electrochemical synthesis of ammonia using ruthenium-platinum alloy at ambient pressure and low temperature[J]. Electrochem. Commun., 2018, 90: 96−100.

[71] Liu G Q, Cui Z Q, Han M M, Zhang S B, Zhao C J, Chen C, Wang G Z, Zhang H M. Ambient electrosynthesis of ammonia on a core-shell-structured Au@CeO_2 catalyst: Contribution of oxygen vacancies in CeO_2[J]. Chem.-Eur. J., 2019, 25(23): 5904−5911.

[72] Wang J, Yu L, Hu L, Chen G, Xin H L, Feng X F. Ambient ammonia synthesis via palladium−catalyzed electrohydrogenation of dinitrogen at low overpotential[J]. Nat. Commun., 2018, 9(1): 1795.

[73] Zhang L L, Cong M Y, Ding X, Jin Y, Xu F F, Wang Y, Chen L, Zhang L X. A janus Fe-SnO_2 catalyst that enables bifunctional electrocatalytic nitrogen fixation[J]. Angew. Chem. Int. Ed, 2020, 59(27): 10888−10893.

[74] Kim K, Yoo C Y, Kim J N, Yoon H C, Han J I. Electrochemical synthesis of ammonia from water and nitrogen in ethylenediamine under ambient temperature and pressure[J]. J. Electrochem. Soc., 2016, 163(14): F1523−F1526.

[75] Li C, Wang T, Zhao Z J, Yang W, Li J F, Li A, Yang Z, Ozin G A, Gong J. Promoted fixation of molecular nitrogen with surface oxygen vacancies on plasmon-enhanced TiO_2 photoelectrodes[J]. Angew. Chem. Int. Ed., 2018, 57(19): 5278−5282.

[76] Zhu D, Zhang L, Ruther R E, Hamers R J. Photo-illuminated diamond as a solid-state source of solvated electrons in water for nitrogen reduction[J]. Nat. Mater., 2013, 12(9): 836−841.

[77] Li M X, Lu Q J, Liu M L, Yin P, Wu C Y, Li H T, Zhang Y Y, Yao S Z. Photoinduced charge separation via the double-electron transfer mechanism in nitrogen vacancies g-C_3N_5/BiOBr for the photoelectrochemical nitrogen reduction[J]. ACS Appl. Mater. Interfaces, 2020, 12(34): 38266−38274.

[78] Li M QC O, Huang H, Low J X, Gao C, Long R, Xiong Y J. Recent progress on electrocatalyst and photocatalyst design for nitrogen reduction[J]. Small Methods, 2018, 3(6): 1673−1674.

[79] Wang Q R, Guo J P, Chen P. Recent progress towards mild-condition ammonia synthesis[J]. J. Energy Chem., 2019, 36: 25−36.

[80] Bai Y J, Bai H Y, Qu K G, Wang F G, Guan P, Xu D B, Fan W Q, Shi W D. In-situ approach to fabricate BiOI photocathode with oxygen vacancies: understanding the N_2 reduced behavior in photoelectrochemical system[J]. Chem. Eng. J., 2019, 362: 349−356.

[81] Ye L Q, Han C Q, Ma Z Y, Leng Y M, Li J, Ji X X, Bi D Q, Xie H Q, Huang Z X. Ni_2P loading on $Cd_{0.5}Zn_{0.5}S$ solid solution for exceptional photocatalytic nitrogen fixation under visible light[J]. Chem. Eng. J., 2017, 307: 311−318.

[82] Ye W, Arif M, Fang X Y, Mushtaq M A, Chen X B, Yan D P. Efficient photoelectrochemical route for the ambient reduction of N_2 to NH_3 based on nanojunctions assembled from MoS_2 nanosheets and TiO_2[J]. ACS Appl. Mater. Inter., 2019, 11(32): 28809−28817.

[83] Lee H K, Koh C SL, Lee Y H, Liu C, Phang I Y, Han X, Tsung C K, Ling X Y. Favoring the unfavored: selective electrochemical nitrogen fixation using a reticular chemistry approach[J]. Sci. Adv., 2018, 4(3): eaar3208.

[84] Wu Z X, Zhao Y, Jin W, Jia B H, Wang J, Ma T Y. Recent progress of vacancy engineering for electrochemical energy conversion related applications[J]. Adv. Funct. Mater., 2021, 31(9): 2009070.

[85] Pan J, Jiang S P. Synthesis of nitrogen doped faceted titanium dioxide in pure brookite phase with enhanced visible light photoactivity[J]. J. Colloid Interface Sci., 2016, 469: 25−30.

[86] Gurylev V, Mishra M, Su C Y, Perng T P. Enabling higher photoelectrochemical efficiency of TiO_2 via controlled formation of a disordered shell: an alternative to the hydrogenation process[J]. Chem. Commun. (Camb.), 2016, 52(48): 7604−7607.

[87] Vu M H, Sakar M, Nguyen C C, Do T O. Chemically bonded Ni cocatalyst onto the S doped g-C_3N_4 nanosheets and their synergistic enhancement in H_2 production under sunlight irradiation[J]. ACS Sustain. Chem. Eng., 2018, 6(3): 4194−4203.

[88] Xiong J, Di J, Xia J X, Zhu W S, Li H M. Surface defect engineering in 2D nanomaterials for photocatalysis[J]. Adv. Funct. Mater., 2018, 28(39): 1801983.

[89] Li H, Shang J, Ai Z H, Zhang L Z. Efficient visible light nitrogen fixation with BiOBr nanosheets of oxygen vacancies on the exposed {001} facets[J]. J. Am. Chem. Soc., 2015, 137(19): 6393−6399.

[90] Wang S Y, Hai X, Ding X, Chang K, Xiang Y G, Meng X G, Yang Z X, Chen H, Ye J H. Light-switchable oxygen vacancies in ultrafine Bi_5O_7Br nanotubes for boosting solar-driven nitrogen fixation in pure water[J]. Adv. Mater., 2017, 29(31): 1701774.

[91] Zhang J Y, Yue L, Zeng Z H, Zhao C R, Fang L J, Hu X, Lin H J, Zhao L H, He Y M. Preparation of $NaNbO_3$ microcube with abundant oxygen vacancies and its high photocatalytic N_2 fixation activity in the help of Pt nanoparticles[J]. J. Colloid Interface Sci., 2023, 636: 480−491.

[92] Lin S, Chen Y H, Fu J J, Sun L, Jiang Q R, Li J F, Cheng J, Lin C J, Tian Z Q. Photoelectrocatalytic nitrogen fixation with V_o-BiOBr/TiO_2 heterostructured photoelectrode as photocatalyst[J]. Int. J. Hydrogen Energy, 2022, 47: 41553−41563.

[93] Zhu M S, Zhai C Y, Sun M J, HuY F, Yan B, Du Y K. Ultrathin graphitic C_3N_4 nanosheet as a promising visible-light-activated support for boosting photoelectrocatalytic methanol oxidation[J]. Appl. Catal. B Environ, 2017, 203: 108−115.

[94] Zhang X D, Yan J, Zheng F Y, Zhao J, Lee L YS. Designing charge transfer route at the interface between WP

nanoparticle and g-C_3N_4 for highly enhanced photocatalytic CO_2 reduction reaction[J]. Appl. Catal. B: Environ., 2021, 286: 119879.

[95] Xie F Y, Dong G F, Wu K C, Li Y F, Wei M D, Du S W. In situ synthesis of g-C_3N_4 by glass-assisted annealing route to boost the efficiency of perovskite solar cells[J]. J. Colloid Interface Sci., 2021, 591: 326−333.

[96] Li G S, Lian Z C, Wang W C, Zhang D Q, Li H X. Nanotube-confinement induced size-controllable g-C_3N_4 quantum dots modified single-crystalline TiO_2 nanotube arrays for stable synergetic photoelectrocatalysis[J]. Nano Energy, 2016, 19: 446−454.

[97] Mohamed H SH, Wu L, Li C F, Hu Z Y, Liu J, Deng Z, Chen L H, Li Y, Su B L. *In-situ* growing mesoporous CuO/O-doped g-C_3N_4 nanospheres for highly enhanced lithium storage[J]. ACS Appl. Mater. Interfaces, 2019, 11(36): 32957−32968.

[98] Chen J J, Mao Z Y, Zhang L X, Wang D J, Xu R, Bie L J, Fahlman B D. Nitrogen-deficient graphitic carbon nitride with enhanced performance for lithium ion battery anodes[J]. ACS Nano, 2017, 11(12): 12650−12657.

[99] Zeng D, Zhou T, Ong W J, Wu M, Duan X, Xu W, Chen Y, Zhu Y A, Peng D L. Sub-5 nm ultra-fine FeP nanodots as efficient co−catalysts modified porous g-C_3N_4 for precious-metal-free photocatalytic hydrogen evolution under visible light[J]. ACS Appl. Mater. Interfaces, 2019, 11(6): 5651−5660.

[100] You Y, Wang S B, Xiao K, Ma T Y, Zhang Y H, Huang H W. Z-scheme g-C_3N_4/Bi_4NbO_8Cl heterojunction for enhanced photocatalytic hydrogen production[J]. ACS Sustain. Chem. Eng., 2018, 6(12): 16219−16227.

[101] Dai J Y, Song J B, Qiu Y, Wei J J, Hong Z Z, Li L, Yang H H. Gold nanoparticle-gecorated g-C_3N_4 nanosheets for controlled generation of reactive oxygen species upon 670 nm laser illumination[J]. ACS Appl. Mater. Interfaces, 2019, 11(11): 10589−10596.

[102] Li Q Y, He L Z, Sun C H, Zhang X W. Computational study of MoN_2 monolayer as electrochemical catalysts for nitrogen reduction[J]. J. Phys. Chem. C, 2017, 121(49): 27563−27568.

[103] Abghoui Y, Skúlason E. Computational predictions of catalytic activity of zincblende (110) surfaces of metal nitrides for electrochemical ammonia synthesis[J]. J. Phys. Chem. C, 2017, 121(11): 6141−6151.

[104] Abghoui Y, Garden A L, Hlynsson V F, Bjorgvinsdottir S, Olafsdottir H, Skulason E. Enabling electrochemical reduction of nitrogen to ammonia at ambient conditions through rational catalyst design[J]. Phys. Chem. Chem. Phys., 2015, 17(7): 4909−4918.

[105] Lv C, Qian Y M, Yan C S, Ding Y, Liu Y Y, Chen G, Yu G H. Defect engineering metal-free polymeric carbon nitride electrocatalyst for effective nitrogen fixation under ambient conditions[J]. Angew. Chem. Int. Ed., 2018, 57(32): 10246−10250.

[106] Spatzal T, Aksoyoglu M, Zhang L, Andrade S L, Schleicher E, Weber S, Rees D C, Einsle O. Evidence for interstitial carbon in nitrogenase FeMo cofactor. Science, 2011, 334(6058): 940.

[107] Lee C C, Hu Y, Ribbe M W. ATP-independent formation of hydrocarbons catalyzed by isolated nitrogenase cofactors[J]. Angew. Chem. Int. Ed., 2012, 51(8): 1947−1949.

[108] Hoffman B M, Lukoyanov D, Yang Z Y, Dean D R, Seefeldt L C. Mechanism of nitrogen fixation by nitrogenase: the next stage[J]. Chem Rev, 2014, 114(8): 4041−4062.

[109] Banerjee A, Yuhas B D, Margulies E A, Zhang Y, Shim Y, Wasielewski M R, Kanatzidis M G. Photochemical nitrogen conversion to ammonia in ambient conditions with FeMoS-chalcogels[J]. J. Am. Chem. Soc., 2015, 137(5): 2030−2034.

[110] Ohki Y, Uchida K, Tada M, Cramer R E, Ogura T, Ohta T. N_2 activation on a molybdenum−titanium−sulfur cluster [J]. Nat. Commun., 2018, 9(1): 3200.

[111] Zhang L, Ji X Q, Ren X, Ma Y J, Shi X F, Tian Z Q, Asiri A M, Chen L, Tang B, Sun X P. Electrochemical ammonia synthesis via nitrogen reduction reaction on a MoS_2 catalyst: theoretical and experimental studies[J]. Adv. Mater., 2018, 30(28): e1800191.

[112] Zhang G H, Yuan X X, Xie B, Meng Y, Ni Z M, Xia S J. S vacancies act as a bridge to peomote electron injection from Z-scheme heterojunction to nitrogen molecule for photocatalytic ammonia synthesis[J]. Cheml. Eng. J., 2022, 433(3): 133670.

[113] Shi Z S, Yang W Q, Gu Y T, Liao T, Sun Z Q. Metal-nitrogen-doped carbon materials as highly efficient catalysts: progress and rational design[J]. Adv. Sci., 2016, 19: 446−454.

[114] Wang S H, Zhan J W, Chen K, Ali A, Zeng L H, Zhao H, Hu W L, Zhu L X, Xu X L. Potassium-doped g-C_3N_4 achieving efficient visible-light-driven CO2 reduction[J]. ACS Sustain. Chem. Eng., 2020, 8(22): 8214−8222.

[115] Zhang Z R, Liu C X, Feng C, Gao P F, Liu Y L, Ren F N, Zhu Y F, Cao C, Yan W S, Si R, Zhou S M, Zeng J. Breaking the local symmetry of $LiCoO_2$ via atomic doping for efficient oxygen evolution[J]. Nano Lett, 2019, 19(12): 8774−8779.

[116] Skulason E, Bligaard T, Gudmundsdottir S, Studt F, Rossmeisl J, Abild-Pedersen F, Vegge T, Jonsson H, Norskov J K. A theoretical evaluation of possible transition metal electro-catalysts for N_2 reduction [J]. Phys. Chem. Chem. Phys., 2012, 14(3): 1235−1245.

[117] Zhao W R, Zhang J, Zhu X, Zhang M, Tang J, Tan M, Wang Y. Enhanced nitrogen photofixation on Fe-doped TiO_2 with highly exposed (101) facets in the presence of ethanol as scavenger[J]. Appl. Catal. B: Environ., 2014, 144: 468−477.

[118] Hu S Z, Chen X, Li Q, Li F Y, Fan Z P, Wang H, Wang Y J, Zheng B H, Wu G. Fe^{3+} doping promoted N_2 photofixation ability of honeycombed graphitic carbon nitride: the experimental and density functional theory simulation analysis[J]. Appl. Catal. B: Environ., 2017, 201: 58−69.

[119] Li X F, Li Q K, Cheng J, Liu L, Yan Q, Wu Y, Zhang X H, Wang Z Y, Qiu Q, Luo Y. Conversion of dinitrogen to ammonia by FeN_3-embedded graphene[J]. J. Am. Chem. Soc., 2016, 138(28): 8706−8709.

[120] Hu S Z, Chen X, Li Q, Li F Y, Fan Z P, Wang H, Wang Y J, Zheng B H, Wu G. Fe^{3+} doping promoted N_2 photofixation ability of honeycombed graphitic carbon nitride: the experimental and density functional theory simulation analysis[J]. Appl. Catal. B: Environ. 2017;(201): 58−69.

[121] Zhang N, Jalil A, Wu D X, Chen S M, Liu Y F, Gao C, Ye W, Qi Z M, Ju H X, Wang C M, Wu X J, Song L, Zhu J F, Xiong Y J. Refining defect states in $W_{18}O_{49}$ by Mo doping: a strategy for tuning N_2 activation towards solar-driven nitrogen fixation[J]. J. Am. Chem. Soc., 2018, 140(30): 9434−9443.

[122] Wang J F, Zhao C R, Yuan S D, Li X J, Zhang J Y, Hu X, Lin H J, Wu Y, He Y M. One-step fabrication of Cu-doped Bi_2MoO_6 microflower for enhancing performance in photocatalytic nitrogen fixation[J]. J. Colloid Interface Sci., 2023, 638: 427−438.

[123] Wang J F, Guan L F, Yuan S D, Zhang J Y, Zhao C R, Hu X, Teng B T, Wu Y, He Y M. Greatly boosted photocatalytic N_2-to-NH_3 conversion by bismuth doping in $CdMoO_4$: band structure engineering and N_2 adsorption modification[J]. Sep. Purif. Technol., 2023, 314: 123554.

[124] Luo Q, Chen L Y, Duan B H, Gu Z Z, Liu J, Xu M L, Duan C Y. Porous N-doped graphitic carbon assembled one-

dimensional hollow structures as high performance electrocatalysts for ORR[J]. RSC Adv, 2016, 6(15): 12467−12471.
[125] Xu F C, Wu F F, Zhu K L, Fang Z P, Jia D M, Wang Y K, Jia G, Low J X, Ye W, Sun Z T. Boron doping and high curvature in Bi nanorolls for promoting photoelectrochemical nitrogen fixation[J]. Appl. Catal. B: Environ., 2021, 284: 119689.
[126] Yu X M, Han P, Wei Z X, Huang L S, Gu Z X, Peng S J, Ma J M, Zheng G F. Boron-doped graphene for electrocatalytic N_2 Reduction[J]. Joule, 2018, 2(8): 1610−1622.
[127] Chen C, Yan D F, Wang Y, Zhou Y Y, Zou Y Q, Li Y F, Wang S Y. BN pairs enriched defective carbon nanosheets for ammonia synthesis with high efficiency[J]. Small, 2019, 15(7): e1805029.
[128] Li H, Shang J, Shi J G, Zhao K, Zhang L Z. Facet-dependent solar ammonia synthesis of BiOCl nanosheets via a proton-assisted electron transfer pathway[J]. Nanoscale, 2016, 8(4): 1986−1993.
[129] Ran J R, Zhang J, Yu J G, Jaroniec M, Qiao S Z. Earth-abundant cocatalysts for semiconductor-based photocatalytic water splitting[J]. Chem. Soc. Rev., 2014, 43(22): 7787−7812.
[130] Ranjit K T, Varadarajan T K, Viswanathan B. Photocatalytic reduction of dinitrogen to ammonia over noble-metal-loaded TiO_2[J]. J. Photochem. Photobiol. A: Chem., 1996, 96(1): 181−185.
[131] Luo M H, Lu P, Yao W F, Huang C P, Xu Q J, Wu Q, Kuwahara Y, Yamashita H. Shape and composition effects on photocatalytic hydrogen production for Pt-Pd alloy cocatalysts[J]. ACS Appl. Mater. Interfaces, 2016, 8(32): 20667−20674.
[132] Qiu P X, Xu C M, Zhou N, Chen H, Jiang F. Metal-free black phosphorus nanosheets-decorated graphitic carbon nitride nanosheets with C-P bonds for excellent photocatalytic nitrogen fixation[J]. Appl. Catal. B: Environ., 2018, 221: 27−35.
[133] Mao C L, Yu L H, Li J, Zhao J C, Zhang L Z. Energy-confined solar thermal ammonia synthesis with K/Ru/$TiO_{2-x}H_x$[J]. Appl. Catal. B: Environ., 2018, 224: 612−620.
[134] Zeng H, Terazono S, Tanuma T. A novel catalyst for ammonia synthesis at ambient temperature and pressure: visible light responsive photocatalyst using localized surface plasmon resonance[J]. Catal. Commun., 2015, 59: 40−44.
[135] Qiu P X, Xu C M, Zhou N, Chen H, Jiang F. Metal-free black phosphorus nanosheets-decorated graphitic carbon nitride nanosheets with C-P bonds for excellent photocatalytic nitrogen fixation[J]. Appl. Catal. B: Environ., 2018, 221: 27−35.
[136] Wang H B, Li H, Zhang M L, Song Y X, Huang J, Huang H, Shao M W, Liu Y, Kang Z H. Carbon dots enhance the nitrogen fixation activity of azotobacter chroococcum[J]. ACS Appl. Mater. Interfaces, 2018, 10(19): 16308−16314.
[137] Li X M, Wang W Z, Jiang D, Sun S M, Zhang L, Sun X. Efficient solar-driven nitrogen fixation over carbon-tungstic-acid hybrids[J]. Chem. Eur. J., 2016, 22(39): 13819−13822.
[138] Oshikiri T, Ueno K, Misawa H. Selective dinitrogen conversion to ammonia using water and visible light through plasmon−induced charge separation[J]. Angew. Chem. Int. Ed., 2016, 55(12): 3942−3946.
[139] Yang J H, Guo Y Z, Jiang R B, Qin F, Zhang H, Lu W Z, Wang J F, Yu J C. High-efficiency "working-in-tandem" nitrogen photofixation achieved by assembling plasmonic gold nanocrystals on ultrathin titania nanosheets[J]. J. Am. Chem. Soc., 2018, 140(27): 8497−8508.
[140] Vu M H, Sakar M, Hassanzadeh-Tabrizi S A, Do T O. Photo(electro)catalytic nitrogen fixation: problems and possibilities[J]. Adv. Mater. Interfaces, 2019, 6(12): 1900091.
[141] Bharath G, Liu C, Banat F, Kumar A, Hai A B, Nadda A K, Gupta V K, Abu Haijia M, Balamurugan. Plasmonic Au nanoparticles anchored 2D WS_2@RGO for high-performance photoelectrochemical nitrogen reduction to ammonia[J]. Chem. Eng. J, 2023, 465: 143040.
[142] Lin S, Ma J B, Fu J J, Sun L, Zhang H, Cheng J, Li J F. Constructing V_o-TiO_2/Ag/TiO_2 heterojunction for efficient photoelectrochemical nitrogen reduction to ammonia[J]. J. Phys. Chem. C, 2023, 127: 1345−1354.
[143] Mei Q F, Zhang F Y, Wang N, Lu W S, Su X T, Wang W, Wu R L. Photocatalysts: Z-scheme heterojunction constructed with titanium dioxide[J]. Chin. J. Inorg. Chem., 2019, 35(8): 1321−1339.
[144] Cao S H, Zhou N, Gao F H, Chen H, Jiang F. All-solid-state Z-scheme 3,4-dihydroxybenzaldehyde-functionalized Ga_2O_3/graphitic carbon nitride photocatalyst with aromatic rings as electron mediators for visible-light photocatalytic nitrogen fixation[J]. Appl. Catal. B: Environ., 2017, 218: 600−610.
[145] Zhao C R, Li X J, Yue L, Yuan S D, Ren X J, Zeng Z H, Hu X, Wu Y, He Y M. One-step preparation of novel Bi-Bi_2O_3/$CdWO_4$ Z-scheme heterojunctions with enhanced performance in photocatalytic NH_3 synthesis[J]. J. Alloy Compd., 2023, 968: 171956.
[146] Yan Z H, Ji M X, Xia J X, Zhu H Y. Recent advanced materials for electrochemical and photoelectrochemical synthesis of ammonia from dinitrogen: one step closer to a sustainable energy future[J]. Adv. Energy Mater., 2019, 10(11): 1902020.

太阳能光（电）催化固氮研究进展

马俊博[a]，林　生[a]，林志群[b]，孙　岚[a,*]，林昌健[a,*]
[a]固体表面物理化学国家重点实验室，化学化工学院化学系，厦门大学，福建 厦门 361005
[b]化学和生物分子工程系，新加坡国立大学，新加坡 117585

摘要

氨（NH_3）是一种现代社会必需的化学物质。目前，工业上合成 NH_3 仍然采用的是 Haber-Bosch 过程，即以 H_2 和 N_2 为反应物在铁基催化剂的作用下于高温（400–600 °C）高压（20–40 Mpa）下将 N_2 转化为 NH_3。然而，其效率只有 10%–15%，同时造成大量的能源消耗，而且 CO_2 排放不可避免。开发构建可持续发展的清洁友好的新能源体系是解决能源危机和环境污染问题、实现碳达峰和碳中和的关键战略。半导体光（电）催化固氮可以利用绿色无污染的太阳能制取重要的基础化工原料氨，有望代替传统的化工制氨工艺，解决其能源消耗严重和环境污染的问题。本文概述了光（电）催化固氮反应及其影响因素、光催化、电催化和光电催化固氮反应实验装置与基本特征、光（电）催化固氮反应催化剂研究进展、光电催化固氮反应机理，着重论述了半导体光催化剂、光（电）催化固氮体系以及光催化固氮机理的最新进展，并对太阳能光催化固氮技术加以评述和展望。

关键词：太阳能；光（电）催化；固氮